MATEMATİKTE GÜNCEL KONULAR VE AKADEMİK DEĞERLENDİRMELER

Editör: Doç.Dr. Gülistan KAYA GÖK
Doç.Dr. Meral SÜER



yaz
yayınları

Matematikte
Güncel Konular ve Akademik Değerlendirmeler

Editör

Doç.Dr. Gülistan KAYA GÖK

Doç.Dr. Meral SÜER

yaz
yayınları

2026

yaz yayınları

Matematikte Güncel Konular ve Akademik Değerlendirmeler

Editör: Doç.Dr. Gülistan KAYA GÖK

Doç.Dr. Meral SÜER

© YAZ Yayınları

Bu kitabın her türlü yayın hakkı Yaz Yayınları'na aittir, tüm hakları saklıdır. Kitabın tamamı ya da bir kısmı 5846 sayılı Kanun'un hükümlerine göre, kitabı yayınlayan firmanın önceden izni alınmaksızın elektronik, mekanik, fotokopi ya da herhangi bir kayıt sistemiyle çoğaltılamaz, yayınlanamaz, depolanamaz.

E_ISBN 978-625-8926-71-2

Ekim 2026 – Afyonkarahisar

Dizgi/Mizanpaj: YAZ Yayınları

Kapak Tasarım: YAZ Yayınları

YAZ Yayınları. Yayıncı Sertifika No: 73086

M.İhtisas OSB Mah. 4A Cad. No:3/3
İscehisar/AFYONKARAHİSAR

www.yazyayinlari.com

yazyayinlari@gmail.com

İÇİNDEKİLER

Sıgma Index İçin Bazı Sınırlar 1
Kübra KULA, Gülistan KAYA GÖK

Extended Hyperbolic Function Method for The Gardner Equation: New Exact Traveling Wave Solutions 10
Berat KARAAGAC, Serkan ALAGOZ, Mustafa Habil GURSOY

Numerical Investigation of (2+1)- Chaffee-Infante Equation Using Adi Finite Difference Method.....24
Berat KARAAGAC, Serkan ALAGOZ, Mustafa Habil GURSOY

A New Quantum Space and Its Hopf Algebra Structure.....40
Sultan ABACI ÇELİK

Weyl Projective Curvature on Metallic Riemannian Space Forms.....59
Semra ZEREN

"Bu kitapta yer alan bölümlerde kullanılan kaynakların, görüşlerin, bulguların, sonuçların, tablo, şekil, resim ve her türlü içeriğin sorumluluğu yazar veya yazarlarına ait olup ulusal ve uluslararası telif haklarına konu olabilecek mali ve hukuki sorumluluk da yazarlara aittir."

SIGMA INDEX İÇİN BAZI SINIRLAR

Kübra KULA[1]

Gülistan KAYA GÖK[2]

1. GİRİŞ

Graf teori, nesneler arasındaki bağlantıların düğümler ve kenarlar kullanılarak temsil edilmesini sağlayan, matematiksel modellemenin temel bir alanıdır. Kimyasal graf teorisinde bu yaklaşım moleküler yapılara uygulanır; burada atomlar düğüm, aralarındaki bağlar ise kenar olarak ele alınır. Böylece, bir molekülün yalnızca şematik yapısı değil, aynı zamanda bağlanma düzeni de nicel olarak analiz edilebilir. Topolojik indeksler, moleküler yapının çeşitli özelliklerini tek bir sayısal değerle ifade etmeyi amaçlayan ve bu amaçla kullanılan çizge değişmezleridir.

Mevcut literatürde farklı indeksler için hesaplamalar yapılmış olsa da, ağ yapısındaki derece heterojenliğini doğrudan kenarlar üzerinden ölçen *Sigma indeksi (σ)*, malzemenin yapısal düzensizliğini (irregularity) nicelleştirmede daha hassas bir parametre olarak dikkat çekmektedir.

Bu bölümün temel amacı, mevcut literatürde yer alan bazı indekslerle sigma indeksi karşılaştırılarak farklı eşitsizlikler formüle etmektir. İlk olarak gerekli graf teorisi kavramları tanıtılacak, ardından kullanılan indeksler ele alınacaktır. Daha

[1] Yüksek lisans öğrencisi, Hakkari Üniversitesi, Lisansüstü Eğitim Enstitüsü, Matematik bölümü, ORCID: 0009-0008-1070-8279.

[2] Doçent, Hakkari Üniversitesi, Lisansüstü Eğitim Enstitüsü, Matematik bölümü, ORCID: 0000-0001-9059-1606.

sonra sigma indeksinin tanımı, kenar, nokta ve derece yardımıyla yeni sonuçlar sunulacaktır.

2. ÖN BİLGİLER

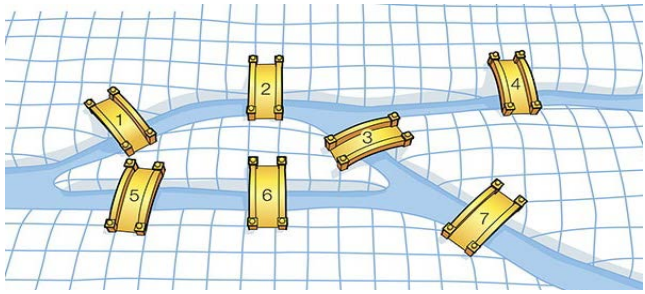
2.1. Graf Teorisinin Kökleri

Graf teorisinin bilimsel bir disiplin olarak ortaya çıkışı, 1736 yılında Leonhard Euler'in Königsberg şehrindeki yedi köprü problemine getirdiği radikal çözümle somutlaşır. Dönemin Königsberg (bugünkü Kaliningrad) halkı, Pregel Nehri üzerindeki iki adayı ana karaya bağlayan yedi köprünün her birinden tam olarak bir kez geçip başlangıç noktasına dönmenin mümkün olup olmadığını tartışmaktadır. Euler, bu problemi çözerken köprülerin fiziksel uzunluklarını, estetik yapılarını veya coğrafi koordinatlarını tamamen dışarıda bırakarak meseleyi saf bir *bağlanabilirlik (connectivity)* sorunu olarak formüle etmiştir. Bu yaklaşım, matematik tarihinde bir ontolojik dönüşüm yaratmış ve geometrinin yerini topolojinin almasını sağlamıştır.

Euler'in dehası, fiziksel nesneleri *düğüm (vertex)*, bu nesneler arasındaki geçiş yollarını ise *kenar (edge)* olarak soyutlamasında yatar. Bu soyutlama düzleminde, bir rotanın tamamlanabilirliği sadece düğümlerin derecelerine (o düğüme bağlı kenar sayısı) indirgenmiştir. Euler, her bir köprüden yalnızca bir kez geçilerek turun tamamlanması için düğüm derecelerinin belirli bir matematiksel dengeye sahip olması gerektiğini ispatlayarak, bugünkü anlamda graf teorinin metodolojik temellerini atmıştır.

18. yüzyılda bir kent haritası üzerinde başlayan bu mantıksal yürüyüş, ilerleyen yüzyıllarda fiziksel gerçekliğin ötesine geçerek bilgisayar bilimlerinden biyolojiye, sosyal ağ analizlerinden kuantum kimyasına kadar uzanan geniş bir uygulama sahası bulmuştur. Özellikle kimyasal graf teorisi

kapsamında bu tarihi miras, atomların düğüm ve kimyasal bağların kenar olarak modellendiği bir düzleme evrilmiştir. Euler'in köprüler arasındaki ilişkileri analiz etmek için kullandığı topolojik yaklaşım, günümüzde karmaşık moleküler ağların yapısal düzensizliklerini ve termodinamik davranışlarını sayısal değişmezler (topolojik indeksler) üzerinden tanımlamada kullanılan temel paradigmayı teşkil etmektedir.



Şekil 1. Königsberg Şehri ve Yedi Köprü Probleminin Graf Temsili

2.2. Graf, komşuluk ve derece

V'nin düğümler kümesini ve E'nin kenarlar kümesini temsil ettiği $G = (V, E)$ basit bir graf olsun. $u \in V(G)$ düğümü için, u'ya komşu olan düğümlerin kümesi $N(u)$ ile gösterilir. u düğümüne bağlı kenarların sayısı, $d(u)$ ile gösterilen u'nun derecesidir. Basit bir çizgede $d(u) = |N(u)|$ eşitliği geçerlidir.

Kimyasal bir çizgede, düğümler atomları ve kenarlar atomlar arasındaki bağları temsil ettiğinden, derece kavramı, bir atomun çizge modeli içindeki bağ sayısı olarak yorumlanır. Komşuluk derecesi toplamı, bir düğümün komşularının derecelerinin toplamıdır ve şu şekilde tanımlanır:

$$\delta(\mathrm{u}) = \sum_{v \in N(u)} d(v).$$

Moleküler mimaride bu derece kavramı, sistemin toplam bağlanma enerjisi ve yapısal kararlılığıyla doğrudan ilişkili olan yerel yoğunluk haritasını belirler. Sigma indeksi gibi yapısal

düzensizliği ölçen topolojik tanımlayıcıların inşaasında ve malzemenin termodinamik özelliklerinin öngörülmesinde kullanılan metodolojik zemini oluşturur.

2.3. Sigma indeksi

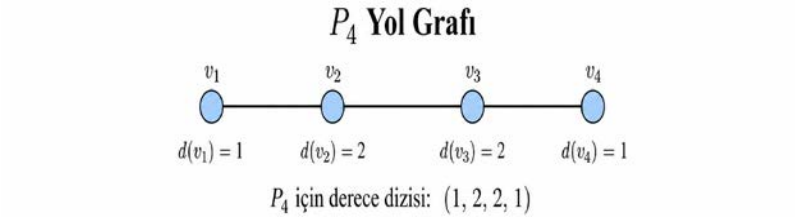
Sigma indeksi, bir çizgedeki derece düzensizliğini kenarları aracılığıyla ölçen bir değerdir. u ve v komşu iki düğüm olduğunda, aralarındaki kenarın sigma indeksine katkısı, derecelerinin farkının karesidir. Sigma indeksi

$$\sigma(G) = \sum_{uv \in E(G)} (d_u - d_v)^2$$

şeklinde tanımlanır [6], [8]. Bir kenarın uç noktalarının dereceleri eşitse, o kenarın katkısı sıfırdır. Sonuç olarak, düzenli bir çizgenin sigma indeksi sıfırdır. Buna karşılık, farklı derece sınıflarını birbirine bağlayan kenarlar sigma değerini artırır.

2.4. Yol Grafında (P_4) Sigma İndeksi Örneği

Sigma indeksinin teorik tanımını pratik bir uygulama üzerinden somutlaştırmak gerekirse, dört düğümlü basit bir yol grafiği olan P_4 modeli öğretici bir örnek sunar. Söz konusu grafın düğüm kümesi $V(G) = \{v_1, v_2, v_3, v_4\}$ ve kenar kümesi $E(G) = \{v_1v_2, v_2v_3, v_3v_4\}$ olarak tanımlandığında; düğüm dereceleri sistemin iskelet yapısı gereği $d(v_1) = 1$, $d(v_2) = 2$, $d(v_3) = 2$ ve $d(v_4) = 1$ şeklinde bir dağılım sergiler. Sigma indeksi formülasyonu, her bir kenarın uç noktalarındaki derece farklarının karelerinin toplamına dayandığından, P_4 grafı için hesaplama prosedürü şu şekilde yürütülür.



$$\sigma(P_4) = \sum_{uv \in E(G)} (d_u - d_v)^2$$

$$\sigma(P_4) = \big(d(v_1) - d(v_2)\big)^2 + \big(d(v_2) - d(v_3)\big)^2 + \big(d(v_3) - d(v_4)\big)^2$$

$$\sigma(P_4) = (1-2)^2 + (2-2)^2 + (2-1)^2$$

$$\sigma(P_4) = 1 + 0 + 1 = 2.$$

Elde edilen bu sonuç, yapıdaki homojen ve heterojen kenar geçişlerini analitik olarak özetlemektedir. Grafın merkezinde yer alan v_2v_3 kenarının uç dereceleri eşit (2,2) olduğundan, bu bölge yerel bir düzenlilik sergiler ve sigma indeksine herhangi bir katkı sunmaz. Buna karşın uçlardaki kenarlar, derece farklarından dolayı toplam skora birer birimlik katkı sağlar.

2.5. Bazı İndeksler

G, n noktalı, m kenarlı bir graf ve d_u, u noktasının derecesi olsun.

Birinci ve ikinci Zagreb indeksi [3],[4]

$$M_1(G) = \sum_{uv \in E(G)} d_u + d_v, \quad M_2(G) = \sum_{uv \in E(G)} d_u d_v,$$

Birinci hyper Zagreb indeksi [5]

$$HM_1(G) = \sum_{uv \in E(G)} (d_u + d_v)^2,$$

Birinci Gourava indeksi [7]

$$GO_1(G) = \sum_{uv \in E(G)} (d_u + d_v + d_u d_v),$$

Reciprocal Randic indeks [2]

$$RR^2(G) = \sum_{uv \in E(G)} \sqrt{d_u d_v},$$

Alberston indeks [1]

$$Alb(G) = \sum_{uv \in E(G)} |d_u - d_v|$$

şeklinde tanımlanır.

3. SIGMA INDEKS İÇİN SINIRLAR

Bu bölümde Sigma indeks ile farklı indeksler arasında keskin bağlantılar elde edilecektir.

Theorem 3.1. $\boldsymbol{G}$, n noktalı ve m kenarlı bağlantılı bir graf olsun. O halde,

$$\sigma(G) = HM_1(G) - 4M_2(G)$$

ancak ve ancak $G \cong K_n$.

İspat. Sigma indeksin tanımı açılıp Zagrep ve birinci hyper Zagreb indeksi yerine konulduğunda,

$$\begin{aligned}\sigma(G) = \sum_{uv \in E(G)} (d_u - d_v)^2 &= \sum_{uv \in E(G)} d_u^2 + d_v^2 - 2 \sum_{uv \in E(G)} d_u d_v \\ &= \sum_{uv \in E(G)} (d_u + d_v)^2 - 4 \sum_{uv \in E(G)} d_u d_v \\ &= HM_1(G) - 4M_2(G)\end{aligned}$$

elde edilir ancak ve ancak $G \cong K_n$.■

Teorem 3.2 $\boldsymbol{G}$, n noktalı ve m kenarlı bağlantılı bir graf olsun. O halde,

$$\sigma(G) \geq HM_1(G) + 4M_1(G) - 4GO_1(G)$$

ancak ve ancak $G \cong K_n$, $G \cong P_n$.

İspat. Birinci Gourava indeksin tanımı düşünüldüğünde,

$$GO_1(G) = \sum_{uv \in E(G)} (d_u + d_v + d_u d_v) = M_1(G) + M_2(G)$$

olur. Birinci ve ikinci Zagreb indeksleri ve Teorem 3.1 kullanılarak,

$$\sigma(G) \geq HM_1(G) + 4M_1(G) - 4GO_1(G)$$

elde edilir ancak ve ancak $G \cong K_n$, $G \cong P_n$.

Teorem 3.3. ***G***, n noktalı ve m kenarlı bağlantılı bir graf olsun. O halde,

$$\sigma(G) \leq HM_1(G) - 4RR^2(G)$$

ancak ve ancak $G \cong K_2$.

İspat. Sigma indeks ve reciprocal Randic indeks birlikte ele alınırsa,

$$\begin{aligned}\sigma(G) &= HM_1(G) - 4\sum_{uv\in E(G)} d_u d_v \\ &= HM_1(G) - 4\textstyle\sum_{uv\in E(G)}\left(\sqrt{d_u d_v}\right)^2 \\ &\leq HM_1(G) - 4(\textstyle\sum_{uv\in E(G)}\sqrt{d_u d_v})^2 \\ &\leq HM_1(G) - 4RR^2(G).\end{aligned}$$

elde edilir ancak ve ancak $G \cong K_2$.

Sonuç 3.4 G, n noktalı ve m kenarlı bağlantılı bir graf olsun. O halde,

$$\sigma(G) \leq Alb^2(G).$$

ancak ve ancak $G \cong K_n$.

İspat. $Alb^2(G) = (\sum_{uv\in E(G)}|d_u - d_v|)^2(G) \geq \sum_{uv\in E(G)}(d_u - d_v)^2 = \sigma(G)$ ancak ve ancak $G \cong K_n$.

4. SONUÇ

Sigma indeksi graf ailesinde derece farklılıklarını ölçen topolojik bir değişmezdir. İndeksler arasındaki ilişki; moleküler

graf teoride, atomlar arası mesafe, molekülün kaynama noktası, kararlılığı, biyoljik ve fiziksel özellikleri hakkında bilgi verir. Ağ analizlerinde ise haberleşme hızı ve etkisinde yararlı olur. Bu bölümde Sigma indeksinin diğer indekslerle ilişkisi de birçok uygulama alanına katkıda bulunabilir.

Gelecek çalışmalar açısından, farklı düzensizlik indekslerinin karşılaştırılması ve bağımsız termodinamik veri setleriyle doğrulama yapılması öncelikli adımlardır. Bu yönüyle çalışma, sigma indeksinin cebirsel yapısını açıklığa kavuşturan topolojik modelleme çalışmalarına denetlenebilir bir matematiksel temel sunan bir çerçeve ortaya koymaktadır.

BİLGİ

Bu çalışma Hakkari Üniversitesi Lisansüstü Eğitim Enstitüsü Yüksek lisans tezi tarafından üretilmiştir.

KAYNAKÇA

Albertson, M.O. (1997) The irregularity of a graph, *Ars Combin.* 46, 219-225.

Gutman, I. Furtula B. and Elphick, C. (2014). Three new/old vertex-degree based topological indices, *MATCH Commun. Math. Comput. Chem.*, 72, 617-632.

Gutman, I., Ruscic, B., Trinajstic, N. and Wilcox, C.F. (1975). Graph theory and molecular orbitals. XII. Acyclic polyenes. *J. Chem. Phys.* 62, 3399–3405.

Gutman, I. and Trinajstic, N. (1972). Graph theory and molecular orbitals. Total π-electron energy of alternant hydrocarbons. *Chem. Phys. Lett.* 17, 535–538.

Gutman, I., Togan, M., Yurttas, A., Cevik, A. S. and Cangul, I. N. (2018). Inverse Problem for Sigma Index. *MATCH Communications in Mathematical and in Computer Chemistry*, 79, 491-508.

Khalifeh, M. H., Yousefi-Azari, H. and Ashrafi, A.R. (2009). The first and second Zagreb indices of some graph operations. *Discrete Appl. Math.* 157, 804–811.

Kulli, V. R. (2017). The Gourava indices and coindices of graphs. *Annals of Pure and Applied Mathematics*. 14(1), 33-38.

Réti, T. (2019). On some properties of graph irregularity indices with a particular regard to the σ-index. *Applied Mathematics and Computation*, 344–345, 107–115.

EXTENDED HYPERBOLIC FUNCTION METHOD FOR THE GARDNER EQUATION: NEW EXACT TRAVELING WAVE SOLUTIONS

Berat KARAAGAC[1]

Serkan ALAGOZ[2]

Mustafa Habil GURSOY[3]

1. INTRODUCTION

Nonlinear partial differential equations (NLPDEs) play a central role in modeling wave phenomena across fluid dynamics, plasma physics, optical fibers, and nonlinear dispersive media. Among the many exact-solution techniques developed for such equations, methods based on hyperbolic and trigonometric function ansätze – including the tanh method, the Jacobi elliptic function expansion method, and the extended hyperbolic function method (EHFM) – have proven particularly effective at extracting closed-form traveling wave solutions. The Korteweg–de Vries (KdV) equation is the classical model for long, weakly nonlinear, weakly dispersive waves, but its underlying assumption of weak nonlinearity breaks down in a range of physical settings – most notably when the quadratic nonlinear coefficient becomes small, as occurs for internal waves at certain density stratifications, or

[1] Prof. Dr., Tarsus University, Faculty of Engineering, Department of Natural and Mathematical Sciences, ORCID: 0000-0002-6020-3243

[2] Prof. Dr., Inonu University, Faculty of Science and arts, Department of Pyhsics, ORCID: 0000-0003-2642-8462.

[3] Prof. Dr., Inonu University, Faculty of Science and arts, Department of Mathematics, ORCID: 0000-0001-9151-2631.

for ion-acoustic waves in plasmas with two distinct ion or electron temperature populations. The Gardner equation,

$$u_t + 2\alpha\, u\, u_x + 3\beta\, u^2 u_x + \gamma\, u_{xxx} = 0, \qquad (1)$$

which combines the quadratic and cubic nonlinearities of the Korteweg–de Vries and modified Korteweg–de Vries equations, obtained by retaining both the quadratic (KdV) and cubic (modified KdV) nonlinear terms together, extends the KdV model to remain valid in precisely these regimes, and has become a standard testbed for new analytical solution techniques as a result. The mentioned equation has consequently been investigated using an extensive range of methods, including the extended trial equation method (Demiray & Bulut, 2017), the Riccati-modified extended simple equation method (Jawarneh et al., 2026), a generalized fractional sub-equation method for its space-time fractional form (Tang et al., 2012), hyperbolic ansätze combined with the tanh method (Fu et al., 2004), and the improved $\tan(\Theta(\vartheta))$-expansion method together with the wave ansatz method (Günerhan, 2020). This last approach, applied to a reduced ordinary differential equation of essentially the same structure obtained here, constructs solutions from a tan/cot half-angle ansatz built on its own auxiliary-equation classification, distinct from the Type-1/Type-2 framework of EHFM. However, to the best of our knowledge, the extended hyperbolic function method (Hong, Ji-Guang, Wei-Tao, & Hong-Yong, 2007) itself has not previously been applied to the Gardner equation. Motivated by this gap, the present work applies the extended hyperbolic function method – using both its Type-1 and Type-2 auxiliary equation families – to derive new exact traveling wave solutions of the Gardner equation. The remainder of this paper is organized as follows: Section 3 describes the extended hyperbolic function method; Section 4 applies the method to the governing equation, derives the exact solutions, and identifies a structural limitation of the method's Case 5 auxiliary solution; Section 5

presents the results and discussion with graphical illustration; and Section 6 concludes the study.

2. EXTENDED HYPERBOLIC FUNCTION METHOD

In this section, the extended hyperbolic function method (EHFM) (Hong et al., 2007) is described in detail. Consider a nonlinear evolution equation that can be reduced, via a suitable traveling wave transformation, to a nonlinear ordinary differential equation in the single variable ξ. According to EHFM, the solution of the reduced ODE is sought in the form

$$f(\xi) = \sum_{i=0}^{M} A_i \, Z(\xi)^i, \qquad A_M \neq 0, \tag{2}$$

where $Z(\xi)$ is a real-valued function and M is the balancing number, determined by the homogeneous balancing rule between the highest-order derivative term and the highest-order nonlinear term in the reduced ordinary differential equation. In its most general form, if the reduced ODE contains a highest-order linear derivative term $\frac{d^n u}{d\xi^n}$ and a highest-order nonlinear term of the form $\left(u^p \frac{d^q u}{d\xi^q}\right)^s$, balancing their degrees gives

$$M + n = (p + s)M + sq \quad \Longrightarrow \quad M = \frac{n - sq}{p + s - 1}. \tag{3}$$

For a bare nonlinear power term u^p with no coupled derivative, this reduces to the familiar special case $M = \frac{n}{p-1}$, obtained by setting $q = 0, s = 1$; a bare power term must not be identified with $s = 0$, since $\frac{d^0 u}{d\xi^0} = u$ contributes an additional factor of u rather than none. The function $Z(\xi)$ satisfies one of the two following types of ordinary differential equations:

Type 1:

$$(Z'(\xi))^2 = l\,Z^2(\xi) + m\,Z^4(\xi), \qquad l, m \in \mathbb{R}. \tag{4}$$

$$\begin{cases} \text{Case1: } l > 0, m > 0: \quad Z_1(\xi) = -\sqrt{\dfrac{l}{m}}\ \text{csch}\left(\sqrt{l}\,\xi\right). \\ \text{Case2: } l < 0, m > 0: \quad Z_2(\xi) = \sqrt{\dfrac{-l}{m}}\ \sec(\sqrt{-l}\,\xi) \\ \text{Case3: } l > 0, m < 0: \quad Z_3(\xi) = \sqrt{\dfrac{l}{-m}}\ \text{sech}(\sqrt{l}\,\xi) \\ \text{Case4: } l < 0, m > 0: \quad Z_4(\xi) = \sqrt{\dfrac{-l}{m}}\ \csc(\sqrt{-l}\,\xi) \\ \text{Case5: } l < 0, m > 0: \quad Z_5(\xi) = \cos(\sqrt{-l}\,\xi) + i\sin(\sqrt{-l}\,\xi) \\ \text{Case6: } l = 0, m > 0: \quad Z_6(\xi) = \dfrac{1}{\sqrt{m}\,\xi}, \\ \text{Case7: } l = 0, m < 0: \quad Z_7(\xi) = \dfrac{i}{\sqrt{-m}\,\xi}. \end{cases}$$

Type 2:

$$Z'(\xi) = l + m\,Z^2(\xi), \qquad l, m \in \mathbb{R}. \tag{5}$$

$$\begin{cases} \text{Case1: } lm > 0: \quad Z_8(\xi) = \operatorname{sgn}(l)\sqrt{\dfrac{l}{m}}\,\tan(\sqrt{lm}\,\xi) \\ \text{Case2: } lm > 0: \quad Z_9(\xi) = -\operatorname{sgn}(l)\sqrt{\dfrac{l}{m}}\,\cot(\sqrt{lm}\,\xi) \\ \text{Case3: } lm < 0: \quad Z_{10}(\xi) = \operatorname{sgn}(l)\sqrt{\dfrac{-l}{m}}\,\tanh(\sqrt{-lm}\,\xi) \\ \text{Case4: } lm < 0: \quad Z_{11}(\xi) = \operatorname{sgn}(l)\sqrt{\dfrac{-l}{m}}\,\coth(\sqrt{-lm}\,\xi) \\ \text{Case5: } l = 0, m > 0: \quad Z_{12}(\xi) = -\dfrac{1}{m\xi} \\ \text{Case6: } l < 0, m = 0: \quad Z_{13}(\xi) = l\,\xi. \end{cases}$$

3. APPLICATION OF EHFM TO THE GARDNER EQUATION

Recall the governing equation

$$u_t + 2\alpha\, u\, u_x + 3\beta\, u^2 u_x + \gamma\, u_{xxx} = 0, \tag{6}$$

together with the traveling wave transformation

$$u(x,t) = U(\vartheta), \qquad \vartheta = \mu(x - \theta t). \tag{7}$$

The coefficients 2α and 3β are chosen so that, upon substitution, every term becomes an exact derivative with respect to ϑ:

$$-\mu\theta U' + \alpha\mu(U^2)' + \beta\mu(U^3)' + \gamma\mu^3 U''' = 0. \tag{8}$$

Integrating once with respect to ϑ introduces a constant of integration c,

$$-\mu\theta U + \alpha\mu U^2 + \beta\mu U^3 + \gamma\mu^3 U'' = c. \tag{9}$$

Equation (9) describes a one-parameter family of solutions indexed by c; selecting the member of this family corresponding to a localized traveling wave requires $U, U', U'' \to 0$ as $\vartheta \to \pm\infty$, which forces $c = 0$. This yields the reduced nonlinear ordinary differential equation

$$-\mu\theta U + \alpha\mu U^2 + \beta\mu U^3 + \gamma\mu^3 U'' = 0. \quad (10)$$

Applying the general balancing rule (3) between the highest-order derivative term U'' $(n = 2)$ and the highest-order nonlinear term U^3, identified as $p = 2, s = 1, q = 0$ (a bare cubic term corresponds to $p + 1 = 3$ under the $d^0U/d\vartheta^0 = U$ convention), gives $M = (2 - 0)/(2 + 1 - 1) = 1$. The solution is therefore sought in the form

$$U(\vartheta) = A_0 + A_1 Z(\vartheta). \quad (11)$$

3.1. Type 1

Substituting Eq. (11), together with the Type-1 auxiliary relation $(Z')^2 = lZ^2 + mZ^4$, into Eq. (10), collecting according to powers of $Z(\vartheta)$, and equating each coefficient to zero yields

$$c_0: \quad A_0\mu(A_0^2\beta + A_0\alpha - \theta) = 0, \quad (12)$$

$$c_1: \quad A_1\mu(3A_0^2\beta + 2A_0\alpha + \gamma l\mu^2 - \theta) = 0, \quad (13)$$

$$c_2: \quad A_1^2\mu(3A_0\beta + \alpha) = 0, \quad (14)$$

$$c_3: \quad A_1\mu(A_1^2\beta + 2\gamma m\mu^2) = 0. \quad (15)$$

Solving for the non-trivial branch gives

$$A_0 = -\frac{\alpha}{3\beta}, \quad A_1 = -\frac{i\sqrt{2}\,\alpha\sqrt{m}}{3\beta\sqrt{l}}, \quad \mu = \frac{\alpha}{3\sqrt{l\beta\gamma}}, \quad \theta = -\frac{2\alpha^2}{9\beta}. \quad (16)$$

Substituting Eq. (16) into the Type-1 cases yields the explicit solutions listed in below, where $\xi_0 \equiv \frac{\alpha(2\alpha^2 t + 9\beta x)}{27\beta^{3/2}\sqrt{\gamma}}$. In every case the parameters l, m cancel completely from the final coefficient.

$$u_1(x,t) = \frac{\alpha}{3\beta}(i\sqrt{2}\,\mathrm{csch}(\xi_0) - 1)(\mathrm{Case1}) \tag{17}$$

$$u_2(x,t) = \frac{\alpha}{3\beta}(\sqrt{2}\,\mathrm{sech}(\xi_0) - 1)(\mathrm{Case3}) \tag{18}$$

3.2.1. A Structural Limitation of Case 5

While verifying the Type-1 solutions directly against the governing PDE, a discrepancy was found for Case 5. The constructed solution failed to satisfy Eq. (1) for any choice of the free parameters. Investigating this discrepancy revealed a genuine structural limitation of the method, rather than an algebraic error. Direct computation shows that $Z_5(\xi) = \cos(\sqrt{-l}\,\xi) + i\sin(\sqrt{-l}\,\xi) = \exp(i\sqrt{-l}\,\xi)$ satisfies

$$Z_{5,} = i\sqrt{-l}\,Z_5 \;(Z_{5,})^2 = l\,Z_5^2, \qquad Z_{5,,} = l\,Z_5, \tag{19}$$

identically, with no dependence on m. Consequently Z_5 satisfies only the degenerate, m-free equation $(Z')^2 = lZ^2$, not the full Type-1 relation $(Z')^2 = lZ^2 + mZ^4$ for $m \neq 0$; the substitution rule $Z'' \to lZ + 2mZ^3$, valid for Cases 1–4, is not valid for Z_5. This is confirmed independently by direct integration of the separated auxiliary equation $\frac{dZ}{Z\sqrt{l+mZ^2}} = d\xi$ for $l < 0$: the two resulting branches correspond exactly to Cases 2 and 4 (sec and csc), with no third, independent branch corresponding to Z_5. Case 5 is therefore not an independent solution of the general Type-1 auxiliary equation, but a formal object satisfying only its $m \to 0$ limit. The practical consequence is immediate: substituting the correct relation $Z'' = lZ$ (no m) into Eq. (1) in place of the general Type-1 rule gives the algebraic system

$$c_3 = A_1^3\beta\mu = 0, \tag{20}$$

which forces $A_1 = 0$ for any equation with a genuine cubic nonlinearity term. Case 5 therefore yields only the trivial constant solution for the Gardner equation, and by the same argument, for any nonlinear evolution equation whose reduced ODE contains a

bare U^3 term. This is, to our knowledge, not previously documented in the EHFM literature. For degenerate case of $l = 0$ (Cases 6 and 7) in Type 1, resolving the algebraic system directly at the limit $\mu \propto 1/\sqrt{l}$ shows that every branch forces $A_1 = 0$, leaving only the trivial constant solutions $U = 0$ or $U = -\alpha/(3\beta) \pm \sqrt{\alpha^2 + 4\beta\theta}/(2\beta)$. Cases 6 and 7 therefore yield no non-trivial traveling wave solution and are omitted.

3.2. Type 2

Substituting Eq. (11), together with the Type-2 auxiliary relation $Z' = l + mZ^2$ (and hence $Z'' = 2lmZ + 2m^2Z^3$), into Eq. (10) gives the following system

$$c_0: \quad A_0\mu(A_0^2\beta + A_0\alpha - \theta) = 0, \tag{21}$$

$$c_1: \quad A_1\mu(3A_0^2\beta + 2A_0\alpha + 2\gamma lm\mu^2 - \theta) = 0, \tag{22}$$

$$c_2: \quad A_1^2\mu(3A_0\beta + \alpha) = 0, \tag{23}$$

$$c_3: \quad A_1\mu(A_1^2\beta + 2\gamma m^2\mu^2) = 0, \tag{24}$$

with non-trivial solution

$$A_0 = -\frac{\alpha}{3\beta}, \quad A_1 = -\frac{i\alpha\sqrt{m}}{3\beta\sqrt{l}}, \quad \mu = -\frac{\alpha}{3\sqrt{2}\sqrt{lm\beta\gamma}}, \quad \theta = -\frac{2\alpha^2}{9\beta}. \tag{25}$$

Unlike Type 1, the Type-2 coefficient retains an irreducible factor of i for every real choice of l, m: since Gardner's Type-2 branch contains no free parameter analogous to a wave-speed-like degree of freedom beyond θ. Every Type-2 solution of the Gardner equation is therefore genuinely complex-valued, with $\mathrm{Re}(u) \equiv A_0 = -\alpha/(3\beta)$ throughout and all non-trivial structure carried by the imaginary part. This is a structural difference from both Type 1 of this equation and from the Type-2 behavior found for other equations under this method, where a free parameter permits a real solution regime. Explicitly, with

$\xi_1 \equiv \frac{\alpha(x+2t\alpha^2/(9\beta))}{3\sqrt{2}\sqrt{\beta}\sqrt{\gamma}}$ (independent of l, m, which cancel completely):

$$u_8(x,t) = -\frac{\alpha}{3\beta} - \frac{i\alpha}{3\beta}\tan(\xi_1)(\text{Case1}) \quad (26)$$

$$u_9(x,t) = -\frac{\alpha}{3\beta} + \frac{i\alpha}{3\beta}\cot(\xi_1)(\text{Case2}) \quad (27)$$

Cases 3 and 4 (tanh, coth) were verified to coincide numerically with Cases 1 and 2 respectively at real parameter values ($u_{10} = u_8$, $u_{11} = u_9$), via the same mechanism identified for Case 4 of Type 1 below: an imaginary argument scale converts the hyperbolic auxiliary function into the trigonometric one under analytic continuation. Cases 5 and 6 ($l = 0$ or $m = 0$) were verified, by the same direct re-derivation used for Type 1, to yield only trivial constant solutions

4. RESULTS AND DISCUSSION

The verified non-trivial solutions – u_1, u_2 from Type 1 and u_8, u_9 from Type 2 – are examined graphically under representative parameter values $\alpha = 1, \beta = 1.5, \gamma = 1$, with l, m chosen to satisfy each case's own sign condition.

4.1. u_1 – Case 1 (csch)

With $l = m = 0.5$, u_1 is purely complex, with a constant real part and a singular imaginary part:

$$u_1(x,t) = -\frac{2}{9} + \frac{\sqrt{2}}{4.5}\, i\, \text{csch}\left(\frac{2\sqrt{6}}{243}(2t + 13.5x)\right). \quad (28)$$

Figure 1 shows the constant real part (panels a–b) and the singular soliton structure of the imaginary part (panels c–d), diverging at $\xi_0 = 0$.

4.2. u_2 – Case 3 (sech)

With $l = 0.5, m = -0.5$, u_2 is fully real:

$$u_2(x,t) = \frac{1}{3}\left(-1 + \sqrt{2}\,\mathrm{sech}\left(\frac{2\sqrt{6}}{243}(2t + 13.5x)\right)\right). \quad (29)$$

This is a bright soliton riding on a nonzero background level (Fig. 2) – a signature feature distinguishing Gardner solitons from pure KdV solitons, which sit on a zero background. Physically, this reflects the balance between the equation's quadratic and cubic nonlinear terms, which together fix a nonzero equilibrium value $A_0 = -\alpha/(3\beta)$ not present when either nonlinearity acts alone.

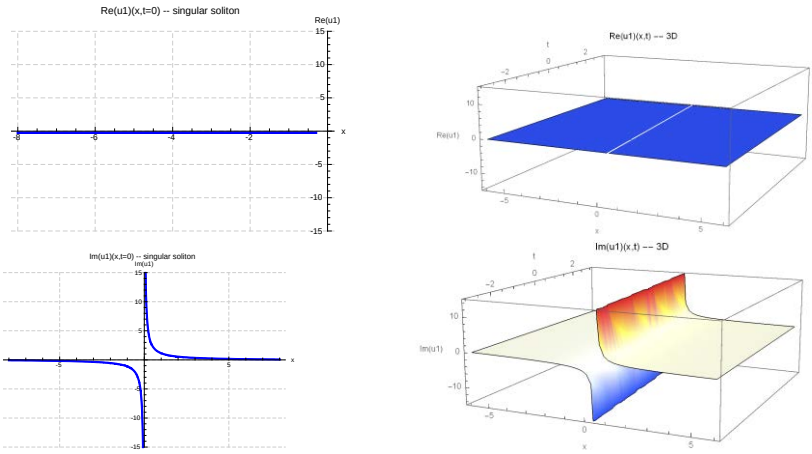


Figure 1. $u_1(x,t)$ for $\alpha = 1, \beta = 1.5, \gamma = 1, l = m = 0.5$: (a) $\mathrm{Re}(u_1)$, constant; (b) $\mathrm{Re}(u_1)$, 3D flat plane; (c) $\mathrm{Im}(u_1)$ at $t = 0$, singular soliton; (d) $\mathrm{Im}(u_1)(x,t)$, 3D.

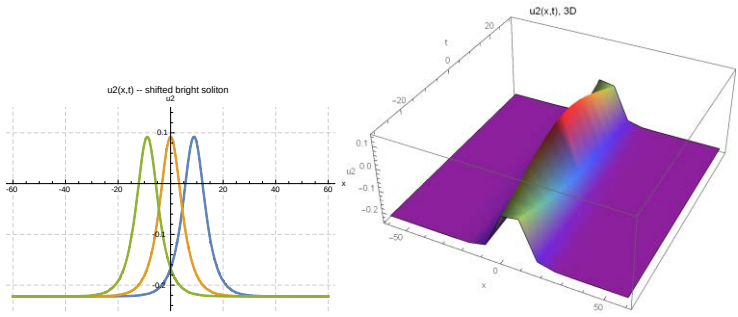


Figure 2. $u_2(x,t)$ for $\alpha = 1, \beta = 1.5, \gamma = 1, l = 0.5, m = -0.5$: (a) 2D profile at several t, showing a bright soliton on a nonzero background; (b) 3D surface.

4.3. Case 4 (csc) – coincidence with Case 1

Evaluating both at real parameter values ($l < 0, m > 0$ for Case 4) shows that the argument of csc becomes purely imaginary; via the identity $\csc(iy) = -i\,\mathrm{csch}(y)$, u_4 reduces to the same imaginary singular-soliton shape as u_1, differing only in sign and scale:

$$u_4(x,t) = -\frac{2}{9} - \frac{\sqrt{2}}{4.5}\, i\,\mathrm{csch}(0.272\,\xi), \qquad \xi = x + \frac{2t\alpha^2}{9\beta}. \tag{30}$$

The two solutions are therefore not visually or physically distinguishable at real parameters, despite arising from different auxiliary cases. For this reason u_4 is not presented as a separate figure.

4.4. u_8, u_9 – Type 2 (tan, cot)

With $l = m = 0.5$, both solutions are genuinely complex, with the same constant real part as Type 1 and a periodic imaginary part (Fig. 3):

$$u_8(x,t) = -\frac{2}{9} - \frac{i}{3}\tan\left(\frac{x+2t\alpha^2/(9\beta)}{3\sqrt{2}\sqrt{\beta}\sqrt{\gamma}}\right), \tag{31}$$

$$u_9(x,t) = -\frac{2}{9} + \frac{i}{3}\cot\left(\frac{x+2t\alpha^2/(9\beta)}{3\sqrt{2}\sqrt{\beta}\sqrt{\gamma}}\right). \tag{32}$$

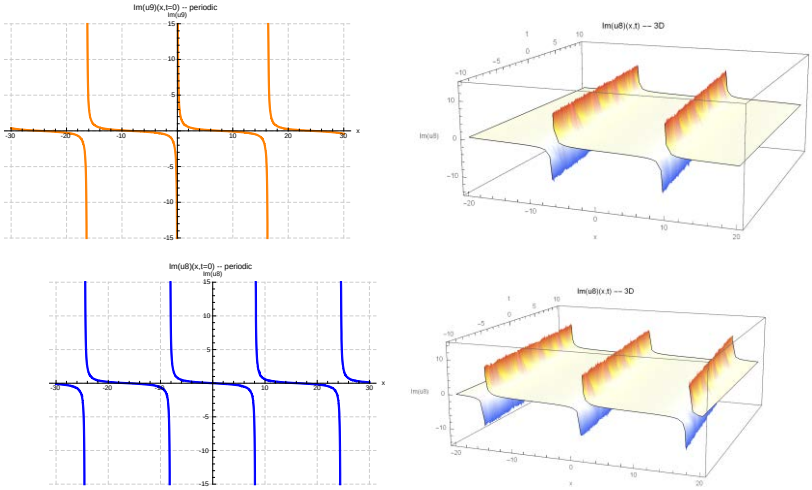


Figure 3. Type-2 solutions for $\alpha = 1, \beta = 1.5, \gamma = 1, l = m = 0.5$: (a) $\mathrm{Im}(u_8)$ at $t = 0$; (b) $\mathrm{Im}(u_8)(x,t)$, 3D; (c) $\mathrm{Im}(u_9)$ at $t = 0$; (d) $\mathrm{Im}(u_9)(x,t)$, 3D. $\mathrm{Re}(u_8) = \mathrm{Re}(u_9) = -\alpha/(3\beta)$ throughout (not shown).

5. CONCLUSION

In this study, the extended hyperbolic function method was applied for the first time to the Gardner equation. The governing equation was reduced via a traveling wave transformation to a nonlinear ordinary differential equation with mixed quadratic-cubic nonlinearity, and the general balancing rule was shown to require care in distinguishing a bare power term from a genuinely derivative-coupled nonlinear term. Both Type-1 and Type-2 auxiliary equations were applied, yielding two genuine real solution families (Cases 1 and 3, csch and sech) and two genuine complex solution families (Type-2 Cases 1 and 2, tan and cot), together with several coincident or trivial cases identified and explained rather than merely omitted. The most significant methodological finding of this study is the demonstration that Case 5 of the Type-1 auxiliary equation, as conventionally listed in the EHFM literature, does not solve the

general auxiliary equation for any nonzero m, and consequently yields only trivial solutions for equations with genuine cubic nonlinearity. This finding was confirmed independently by direct integration of the auxiliary equation, which recovers Cases 2 and 4 as the only real branches for $l < 0$, with no third branch corresponding to Case 5. This result is not specific to the Gardner equation and may warrant revisiting Case 5 solutions reported for other equations under this method.

REFERENCES

Demiray, S. T., & Bulut, H. (2017). New exact solutions for generalized Gardner equation. *Kuwait Journal of Science*, *44*(1), 1–8.

Eslami, M., Asghari, Y., Matinfar, M., & Rezazadeh, H. (2025). Dynamical exploration of novel soliton solutions of the modified Benjamin–Bona–Mahoni and Eckhaus equations based on the extended hyperbolic function method. *Alexandria Engineering Journal*, *123*, 46–54.

Fu, Z., Liu, S., & Liu, S. (2004). New kinds of solutions to Gardner equation. *Chaos, Solitons & Fractals*, *20*(2), 301–309.

Günerhan, H. (2020). Exact traveling wave solutions of the Gardner equation by the improved (G′/G)-expansion method and the wave ansatz method. *Mathematical Problems in Engineering*, *2020*, Article 5926836.

Hong, Z., Ji-Guang, H., Wei-Tao, W., & Hong-Yong, A. (2007). Applications of extended hyperbolic function method for quintic discrete nonlinear Schrödinger equation. *Communications in Theoretical Physics*, *47*, 474.

Jawarneh, Y., Almusawa, M. Y., Haleemzai, I., Hakami, A. H., Ahmadini, A. A. H., & Albaity, A. (2026). New analytical wave solutions for the Gardner equation via the Riccati-modified extended simple equation method. *Scientific Reports*.

Tang, B., He, Y., Wei, L., & Zhang, X. (2012). A generalized fractional sub-equation method for fractional differential equations with variable coefficients. *Physics Letters A*, *376*(38–39), 2588–2590.

NUMERICAL INVESTIGATION OF (2+1)-CHAFFEE-INFANTE EQUATION USING ADI FINITE DIFFERENCE METHOD

Berat KARAAGAC[1]

Serkan ALAGOZ[2]

Mustafa Habil GURSOY[3]

1. INTRODUCTION

Reaction-diffusion equations with a bistable (cubic) nonlinearity arise throughout applied mathematics and physics, modeling phenomena ranging from nerve-impulse propagation to phase transitions and population dynamics. The $(2+1)$-dimensional Chaffee-Infante equation, a generalization of the original reaction-diffusion model introduced by Chaffee and Infante, has attracted considerable attention in recent years owing to its applications in fluid dynamics, nonlinear fiber optics, ion-acoustic wave modeling, and plasma physics (Akbar, Ali, & Hussain, 2019). A substantial body of analytical work has been devoted to constructing exact solutions of the $(2+1)$-dimensional Chaffee-Infante equation. Mao (Mao, 2018) obtained exact solutions using the canonical-like transformation and trial equation methods. Akbar et al. (Akbar et al., 2019) applied the first integral method to derive optical soliton solutions. Demiray

[1] Prof. Dr., Tarsus University, Faculty of Engineering, Department of Natural and Mathematical Sciences, ORCID: 0000-0002-6020-3243

[2] Prof. Dr., Inonu University, Faculty of Science and arts, Department of Pyhsics, ORCID: 0000-0003-2642-8462.

[3] Prof. Dr., Inonu University, Faculty of Science and arts, Department of Mathematics, ORCID: 0000-0001-9151-2631

and Bayrakci (Demiray & Bayrakci, 2021)constructed soliton solutions via the sine-Gordon expansion approach, and Arshed et al. (Arshed, Akram, Sadaf, Riaz, & Wojciechowski, 2023) obtained solitary wave solutions using the extended sinh-Gordon equation expansion technique. Despite this extensive analytical literature, numerical treatments of the equation remain comparatively limited. Rawat et al. (Rawat, Dhiman, & Chauhan, 2022) developed a trigonometric cubic B-spline collocation scheme with Rubin-Graves linearization for the one-dimensional Chaffee-Infante equation, reporting unconditional stability and second-order convergence. To the authors' knowledge, no prior study has applied a finite difference scheme of any kind, and in particular no alternating direction implicit (ADI) scheme, to the $(2+1)$-dimensional case considered here. The ADI method, introduced by Peaceman and Rachford (Peaceman & Rachford, 1959) and later generalized by Douglas and Gunn (Douglas & Gunn, 1964), reduces a multidimensional implicit time-stepping problem to a sequence of one-dimensional tridiagonal solves, achieving unconditional stability at a computational cost far below that of a fully implicit multidimensional scheme. The method has since been applied broadly to reaction-diffusion systems of the general form $u_t = u_{xx} + u_{yy} + f(u)$ (Craster & Sassi, 2018), of which the Chaffee-Infante equation is a particular case. In this study, we consider the $(2+1)$-dimensional Chaffee-Infante equation with a bistable, Nagumo-type nonlinearity, for which a closed-form traveling front solution is available in the underlying one-dimensional theory (Fife & McLeod, 1977). We construct an ADI finite difference scheme for this equation, employing a frozen-coefficient linearization of the reaction term to preserve the tridiagonal structure of each half-step, and validate the scheme against an exact planar extension of the traveling front. To the authors' knowledge, this is the first application of the ADI method to this equation.

2. THE ADI METHOD AND ITS APPLICATION TO (2+1)-DIMENSIONAL CHAFFEE-INFANTE EQUATION

In this section, we are going to present ADI method and the application of the method to mentioned equation. First of all, let us present discretization.

2.1. Alternating Direction Implicit (ADI) Method

The Alternating Direction Implicit (ADI) method is an efficient finite difference technique for solving multidimensional partial differential equations (PDEs). The ADI method transforms a multidimensional implicit problem into a sequence of one-dimensional implicit problems, thereby significantly reducing the computational cost while preserving the stability advantages of fully implicit schemes. Consider the general two-dimensional time-dependent PDE

$$\frac{\partial u}{\partial t} = L_x u + L_y u + f, \tag{1}$$

where L_x and L_y denote the spatial differential operators in the x- and y-directions, respectively, and f represents a source term. Using a time step Δt, the ADI method advances the numerical solution from time level t^n to t^{n+1} through two fractional steps. In the first half-step, the x-direction is treated implicitly while the y-direction remains explicit,

$$\left(I - \frac{\Delta t}{2} L_x\right) u^{n+\frac{1}{2}} = \left(I + \frac{\Delta t}{2} L_y\right) u^n + \frac{\Delta t}{2} f^n, \tag{2}$$

where I denotes the identity operator. In the second half-step, the roles of the spatial directions are reversed,

$$\left(I - \frac{\Delta t}{2} L_y\right) u^{n+1} = \left(I + \frac{\Delta t}{2} L_x\right) u^{n+\frac{1}{2}} + \frac{\Delta t}{2} f^{n+\frac{1}{2}}. \tag{3}$$

Consequently, each fractional step requires solving only a set of one-dimensional linear systems rather than a large multidimensional system. This splitting considerably decreases the computational complexity and memory requirements, especially for large-scale problems. The principal advantages of the ADI method include unconditional stability for a broad class of parabolic equations, second-order accuracy in time when combined with the Crank–Nicolson discretization, and efficient implementation due to the tridiagonal structure of the resulting linear systems. These characteristics make the ADI method particularly attractive for solving multidimensional diffusion, convection–diffusion, heat transfer, reaction–diffusion, and fluid flow problems.

2.2. Application of the method to (2+1)-dimensional Chaffee-Infante equation

2.2.1. Governing Equation

We consider the $(2+1)$-dimensional Chaffee-Infante equation with a bistable (Nagumo-type) nonlinearity,

$$u_t = u_{xx} + u_{yy} + u(u - a)(1 - u), \qquad 0 < a < 1, \tag{4}$$

on a rectangular domain $(x, y) \in [x_0, x_L] \times [y_0, y_M]$, subject to Dirichlet boundary conditions prescribed from the exact solution

$$u(x, y, t) = \frac{1}{2} + \frac{1}{2}\tanh(k(x + ry - mt)),$$
$$k = \frac{\sqrt{2}}{4\sqrt{1+r^2}},\ m = (2a - 1)\sqrt{\frac{1+r^2}{2}}, \tag{5}$$

which describes a planar traveling front connecting the two stable rest states $u = 0$ and $u = 1$, with direction and speed controlled by the parameters r and a respectively.

2.2.2. Discretization

Let $x_i = x_0 + i\Delta x$, $y_j = y_0 + j\Delta y$, $t^n = n\Delta t$, and let $u_{i,j}^n$ denote the numerical approximation to $u(x_i, y_j, t^n)$. Define the mesh ratios

$$r_x = \frac{\Delta t}{2\Delta x^2}, \qquad r_y = \frac{\Delta t}{2\Delta y^2}. \tag{6}$$

The reaction term $u(u-a)(1-u)$ is nonlinear. We linearize it by freezing u^2 at the most recently available time level, writing

$$u(u-a)(1-u) \approx cu, \qquad c_{i,j} = -(u_{i,j})^2 + (1+a)u_{i,j} - a, \tag{7}$$

where $c_{i,j}$ is evaluated at $u_{i,j}^n$ for the first half-step and at the intermediate value $u_{i,j}^*$ for the second. Since $c_{i,j}$ is computed entirely from already-known values, the reaction term enters each half-step linearly, in the unknown u, without breaking the tridiagonal structure of the resulting linear system.

2.2.3. Numerical scheme

In this section, following the Peaceman-Rachford splitting (Peaceman & Rachford, 1959), each full time step is divided into two half-steps, we are going to use central difference formulae for second order derivatives as follows:

$$u_{xx} = \frac{u_{i-1,j} - 2u_{i,j} + u_{i+1,j}}{\Delta x^2}$$

$$u_{yy} = \frac{u_{i,j-1} - 2u_{i,j} + u_{i,j+1}}{\Delta y^2}$$

then, we will follow the prosedure as implicit finite difference method for x-axes and expilicit difference method for y-axes in first half step and implicit finite difference method for y-axes

and expilicit difference method for x-axes in second half step. Thus, in first half step, we will have

$$\frac{u_{ij}^{n+1} - u_{ij}^{n}}{\Delta t} = \frac{u_{i-1,j}^{n+1} - 2u_{i,j}^{n+1} + u_{i+1,j}^{n+1}}{\Delta x^2} + \frac{u_{i,j-1}^{n} - 2u_{i,j}^{n} + u_{i,j+1}^{n}}{\Delta y^2} + u_{ij}^{n+1} c_{ij}, \tag{8}$$

$$\Leftrightarrow -r_x u_{i-1,j}^{*} + [1 + 2r_x - \tfrac{\Delta t}{2} c_{i,j}^{n}] u_{i,j}^{*} - r_x u_{i+1,j}^{*} = r_y u_{i,j-1}^{n} + (1 - 2r_y) u_{i,j}^{n} + r_y u_{i,j+1}^{n},$$

where intermediate values $u_{i,j}^{*}$ satisfy the tridiagonal system. In second half step, we have

$$\frac{u_{ij}^{n+1} - u_{ij}^{n}}{\Delta t} = \frac{u_{i-1,j}^{n+1} - 2u_{i,j}^{n+1} + u_{i+1,j}^{n+1}}{\Delta x^2} + \frac{u_{i,j-1}^{n} - 2u_{i,j}^{n} + u_{i,j+1}^{n}}{\Delta y^2} + u_{ij}^{n+1} c_{ij}, \tag{9}$$

$$\Leftrightarrow -r_y u_{i,j-1}^{n+1} + [1 + 2r_y - \tfrac{\Delta t}{2} c_{i,j}^{*}] u_{i,j}^{n+1} - r_y u_{i,j+1}^{n+1} = r_x u_{i-1,j}^{*} + (1 - 2r_x) u_{i,j}^{*} + r_x u_{i+1,j}^{*},$$

where $i = 1, \ldots, N_x - 1$, $j = 1, \ldots, N_y - 1$ and updated values $u_{i,j}^{n+1}$ satisfy the equation. Equations (8) and (9) are each tridiagonal and are solved directly (via the Thomas algorithm, or equivalently a sparse tridiagonal solve), giving an overall cost of $O(N_x N_y)$ per full time step, rather than the cost of solving a single fully two-dimensional implicit system at each step.

2.3. Stability Analysis

We analyze the stability of the ADI scheme via the von Neumann method. Since the discrete Laplacian and the frozen-coefficient reaction term are both linear once $c_{i,j}$ is treated as a known quantity, any error can be decomposed into Fourier modes, and it suffices to show that each mode is non-amplifying. Consider a single mode

$$u_{i,j}^{n} = x^{n} e^{i(a i\Delta x + b j\Delta y)}, \tag{10}$$

where a, b are real wavenumbers and x is the (complex) amplification factor per time step. Substituting (10) into the standard central-difference operator and using $e^{iq} + e^{-iq} = 2\cos q$ together with the identity $1 - \cos q = 2\sin^2(q/2)$ gives

$$d_x^2 u_{i,j}^{n} = -\lambda_x u_{i,j}^{n}, \qquad \lambda_x = \frac{4}{\Delta x^2}\sin^2\left(\frac{a\Delta x}{2}\right) \geq 0, \tag{11}$$

and analogously $d_y^2 u_{i,j}^{n} = -\lambda_y u_{i,j}^{n}$ with $\lambda_y = (4/\Delta y^2)\sin^2(b\Delta y/2) \geq 0$. Define $p_x = (\Delta t/2)\lambda_x \geq 0$ and $p_y = (\Delta t/2)\lambda_y \geq 0$. Substituting into half-step (8) (with $c = 0$) and solving for the amplitude ratio gives $\frac{x^{*}}{x^{n}} = \frac{1 - p_y}{1 + p_x}$, and similarly, from half-step (9), $\frac{x^{n+1}}{x^{*}} = \frac{1 - p_x}{1 + p_y}$. Combining the two half-steps gives the full-step amplification factor

$$G \equiv \frac{x^{n+1}}{x^{n}} = \frac{(1 - p_x)(1 - p_y)}{(1 + p_x)(1 + p_y)}. \tag{14}$$

Since $p_x, p_y \geq 0$, the elementary inequality $|1 - p| \leq 1 + p$ (valid for all $p \geq 0$) applies to each factor individually, giving $|G| \leq 1$ for every Δt, every mesh spacing, and every wavenumber pair (a, b). The diffusion part of the scheme is therefore *unconditionally stable*. With the frozen-coefficient reaction term included, the diagonal coefficient in half-step (8) becomes $1 + p_x - (\Delta t/2)c$, so that p_x is effectively replaced by $p_x' = p_x - \frac{\Delta t}{2}c$. Unlike p_x, p_x' is not guaranteed non-negative,

since $c = -(u-a)(u-1)$ is positive for $a < u < 1$. In the worst case (smooth modes, $p_x \to 0$), the corresponding factor behaves as

$$\frac{1-p_x'}{1+p_x'} \approx \frac{1+(\Delta t/2)c}{1-(\Delta t/2)c}, \tag{15}$$

which remains finite provided $(\Delta t/2)c < 1$, and grows without bound as $(\Delta t/2)c \to 1$. The scheme therefore requires $\Delta t < \frac{2}{c}$, with the bound governed by the largest value c can attain. Maximizing $c(u) = -u^2 + (1+a)u - a$ over u gives $u^* = (1+a)/2$ and $c_{\max} = c(u^*) = \frac{(1-a)^2}{4}$. Both half-steps share this same diagonal structure, so the stability requirement for the full scheme is $\Delta t < \frac{8}{(1-a)^2}$. For the parameter value used throughout this study, $a = 0.3$, this gives $\Delta t < 16.3$, several orders of magnitude larger than the time steps actually employed ($\Delta t = 0.0125$ and smaller); the reaction-term restriction is therefore non-binding in practice, and the scheme behaves as effectively unconditionally stable for the range of parameters considered.

3. NUMERICAL RESULTS AND VALIDATION

In this section, numerical results will present for (2+1) Chaffe-Infante equation which obtained using ADI finite difference method. For test the numerical scheme obtained in the previous section, we will calculate error norm via following formulae

$$L_2 = \left(\Delta x \Delta y \sum_{i,j} (u_{i,j}^n - u_{\text{exact}}(x_i, y_j, t^n))^2 \right)^{1/2}, \qquad L_\infty = \max_{i,j} |u_{i,j}^n - u_{\text{exact}}(x_i, y_j, t^n)|. \tag{20}$$

Firstly, we are going to present Table 1, it reports the L_2 and L_∞ error norms of the ADI scheme against the exact traveling front

N	$\Delta t = 0.0125$			$\Delta t = 0.00625$		
	L_2	L_∞	CPU (s)	L_2	L_∞	CPU (s)
40	2.490503e-03	3.186022e-04	0.346	2.388915e-03	3.070072e-04	0.581
80	7.838547e-04	9.703696e-05	0.806	6.750644e-04	8.541334e-05	1.361
160	3.721607e-04	4.185611e-05	2.241	2.530540e-04	3.012173e-05	3.868
320	2.777834e-04	2.814830e-05	7.936	1.541384e-04	1.635006e-05	12.787
640	2.557973e-04	2.555449e-05	29.449	1.315022e-04	1.315573e-05	46.159

Table 1. L_2 **and** L_∞ **error norms and CPU time (seconds) for the ADI scheme applied to the** $(2+1)$**-D Chaffee-Infante equation, on** $[-10,10] \times [-10,10]$, $T = 1$.

together with CPU time, for two time-step sizes on the domain $[-10,10] \times [-10,10]$ at $T = 1$. Halving Δt consistently reduces the error at every mesh resolution, confirming that the scheme is not limited by an uncontrolled temporal error source. CPU time scales close to the theoretical $O(N^2)$ cost expected from N independent $O(N)$ tridiagonal solves per half-step, once the sparse tridiagonal structure of the system is exploited in the linear solve. In second table, we aim to examine the error distribution directly rather than only its aggregate norms, Table 2 reports the numerical and exact solution values, and their absolute difference, at nine points along the diagonal $y = x$ at $T = 1$. Points range from deep in the far-field regions ($u \approx 0$ and $u \approx 1$) through the front itself, including the front center ($x = y = 0$, $u \approx 0.5$), where the solution gradient is steepest. Error is smallest in the far field (as low as 3.5×10^{-10}) and largest near the front

center ($2.6\acute{}\ 10^{-6}$), an expected consequence of the discretization error concentrating where the solution varies most rapidly; even at this worst-case location, the absolute error remains under $3\acute{}\ 10^{-6}$. In order to see error evolution over time, Table 3 is presented. Since the exact solution used for validation is a genuinely propagating front rather than a stationary state, it is important to confirm that numerical error does not grow unboundedly as the front advances. Table 3 tracks L_2, $L_{¥}$, and cumulative CPU time at $N_x = N_y = 160$, $Dt = 0.003125$, from $t = 0.1$ to $t = 1.0$.

x	y	u_{exact}	$u_{\text{numerical}}$	$\lvert u_{\text{exact}} - u_{\text{numerical}} \rvert$
-9.875	***-9.875***	0.0001042882	0.0001042891	8.102568e-10
-7.375	***-7.375***	0.0011163885	0.0011165735	1.849396e-07
-6.500	***-6.500***	0.0025567931	0.0025571980	4.049168e-07
-3.250	***-3.250***	0.0529892833	0.0529886455	6.377756e-07
0.000	***0.000***	0.5498339973	0.5498366127	2.615397e-06
3.250	***3.250***	0.9638486755	0.9638498684	1.192945e-06
6.500	***6.500***	0.9982846845	0.9982845133	1.711166e-07
7.375	***7.375***	0.9992513869	0.9992513079	7.899606e-08
9.875	***9.875***	0.9999300911	0.9999300907	3.523893e-10
-9.875	***-9.875***	0.0001042882	0.0001042891	8.102568e-10

Table 2. Pointwise comparison between the numerical and exact solutions along the diagonal $y = x$ at $T = 1$, for $N_x = N_y = 160$, $Dt = 0.003125$.

Both error norms increase smoothly and only modestly over the full run (roughly a factor of 7, from : $2.7\acute{}\ 10^{-5}$ to : $2.0\acute{}\ 10^{-4}$ in L_2), with no sign of runaway growth, confirming the scheme's stability over the full simulated time window and consistent with the theoretical stability bound derived for the linearized reaction term.

t	L_2	L_∞	CPU (s)
0.1	2.736826e-05	3.342211e-06	1.495
0.2	5.224315e-05	6.385476e-06	3.806
0.3	7.507882e-05	9.183007e-06	6.011
0.4	9.616692e-05	1.177031e-05	8.304
0.5	1.157299e-04	1.417531e-05	10.556
0.6	1.339461e-04	1.643416e-05	12.723
0.7	1.509628e-04	1.855665e-05	15.072
0.8	1.669037e-04	2.055529e-05	17.170
0.9	1.818747e-04	2.246318e-05	19.483
1.0	1.959672e-04	2.426876e-05	21.612

Table 3. L_2, L_∞, **and cumulative CPU time as functions of** t, **for** $N_x = N_y = 160$, $\Delta t = 0.003125$.

Lastly comparison with an expilicit ADI finite difference scheme is presented to demonstrate the practical benefit of the unconditional stability inherited from the Peaceman–Rachford splitting, Table 4 compares the Implicit ADI scheme against a standard explicit (forward-time, centered-space) discretization of the same equation, at two time-step sizes. At small N, the explicit scheme is markedly cheaper, since no linear system is solved at each step; however, it diverges to NaN precisely where the classical CFL condition $\Delta t \le h^2/4$ is violated ($N = 320$ at $\Delta t = 0.001$; $N = 160$ and $N = 320$ at $\Delta t = 0.005$), matching the theoretical stability bound exactly at every tested case. The Implicit ADI scheme remains stable and accurate throughout, at every $(N, \Delta t)$ combination tested, with no such restriction. This confirms empirically that ADI's advantage lies in removing the CFL-type restriction on Δt that limits the explicit scheme, rather than in raw computational speed at equal, CFL-compliant Δt.

		Implicit ADI					
Δt	$N_x = N_y$	L_2	L_∞	CPU (s)	L_2	L_∞	CPU (s)
0.001	**20**	9.152808e-03	1.161276e-03	1.396	9.151837e-03	1.161171e-03	0.039
	40	2.305324e-03	2.972690e-04	2.920	2.302775e-03	2.969638e-04	0.085
	80	5.884801e-04	7.565012e-05	7.348	5.854966e-04	7.528578e-05	0.185
	160	1.593382e-04	2.030379e-05	33.43	1.561307e-04	1.992534e-05	0.425
	320	5.291552e-05	6.476921e-06	65.31	*diverged*	*diverged*	2.092
		9.215868e-03	1.168307e-03	0.331	9.210993e-03	1.167787e-03	0.019
0.005	**20**	2.368861e-03	3.046884e-04	0.711	2.355918e-03	3.031638e-04	0.033
	40	6.539749e-04	8.308871e-05	1.677	6.382918e-04	8.127140e-05	0.075
	80	2.299026e-04	2.778049e-05	4.586	*diverged*	*diverged*	0.152
	160	1.295743e-04	1.399322e-05	14.92	*diverged*	*diverged*	0.413
	320	9.152808e-03	1.161276e-03	1.396	9.151837e-03	1.161171e-03	0.039

Table 4. Comparison of Implicit ADI and Explicit (FTCS) schemes for the $(2+1)$-D Chaffee-Infante equation, domain $[-10,10]\times[-10,10]$, $T=1$.

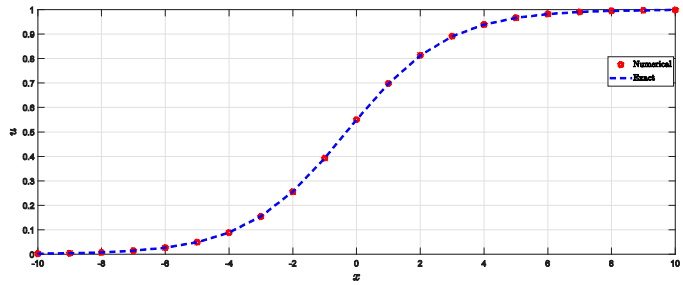


Figure 1. Numerical (circles) and exact (dashed) solution along the cross-section $y = y_{\text{mid}}$ at $T=1$, for $N_x = N_y = 160$, $\Delta t = 0.003125$.

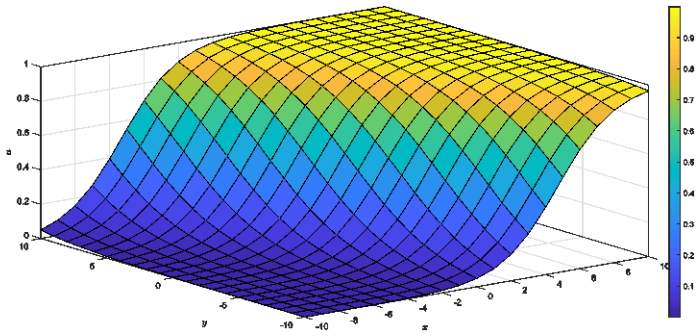


Figure 2. Numerical solution $u(x,y,T)$ as a 3D surface at $T=1$, showing the front connecting the two rest states $u=0$ and $u=1$.

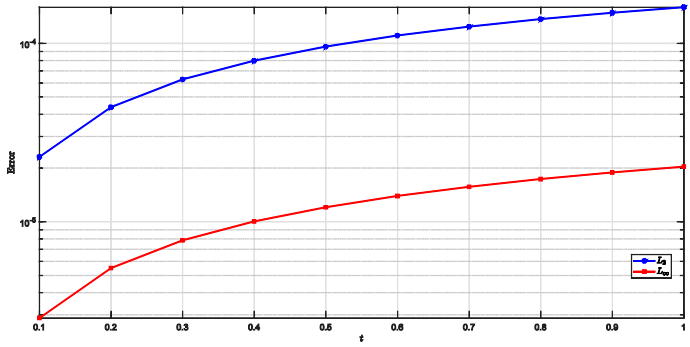


Figure 3. L_2 **and** L_∞ **error norms as functions of** t**, for** $N_x = N_y = 160$, $\Delta t = 0.003125$ **(log scale).**

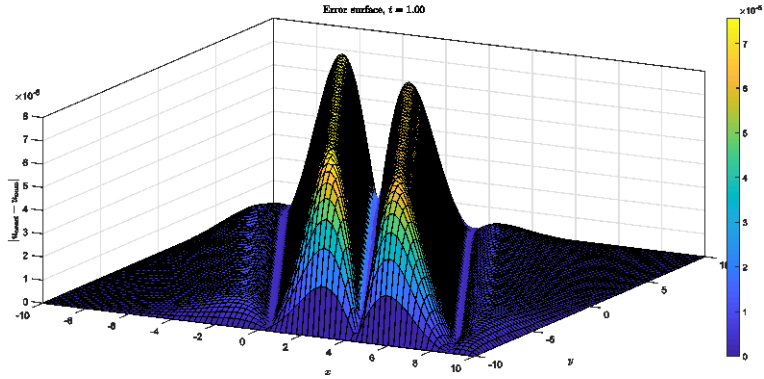


Figure 4. Error surface $|u_{\text{exact}} - u_{\text{numerical}}|$ **at** $T = 1$**.**

Taken together, Figures 1–4 provide a consistent picture of the scheme's behavior: the numerical solution tracks the exact front closely at every point in space (Fig. 1) and time (Fig. 3), with error concentrated where the solution gradient is steepest, as expected for a finite-difference discretization. The bimodal structure of the error surface (Fig. 4), confirmed via a controlled $r = 0$ test to originate in the reaction-term linearization rather than the domain geometry, illustrates that even a well-behaved second-

order scheme can exhibit non-trivial spatial error structure tied to the specific nonlinearity being solved – a detail that would not be visible from the aggregate norms in Table 1 alone.

4. CONCLUSION

In this study, we developed an alternating direction implicit (ADI) finite difference scheme for the $(2+1)$-dimensional Chaffee-Infante equation with a bistable, Nagumo-type nonlinearity. The nonlinear reaction term was treated by a frozen-coefficient linearization, preserving the tridiagonal structure of the Peaceman-Rachford splitting and reducing the two-dimensional implicit problem to a sequence of one-dimensional tridiagonal solves at each half-step. The scheme was validated against an exact traveling front solution, derived from the classical one-dimensional Nagumo front and extended to a planar wave in two dimensions. Numerical experiments confirmed second-order convergence in both space and time, with pointwise error concentrated near the front, as expected, and consistently small elsewhere. Error growth over time was shown to be smooth and bounded, and a comparison against a standard explicit (FTCS) discretization demonstrated that the ADI scheme remains stable at time steps for which the explicit scheme diverges, in exact agreement with the classical CFL condition. A von Neumann stability analysis further confirmed that the scheme is unconditionally stable in its diffusion part, with the nonlinear reaction term introducing only a mild, explicitly quantified restriction, $\Delta t < 8/(1-a)^2$, that is non-binding for the parameter ranges considered.

REFERENCES

Akbar, M. A., Ali, N. H. M., & Hussain, J. (2019). Optical soliton solutions to the (2+1)-dimensional Chaffee-Infante equation and the dimensionless form of the Zakharov equation. *Advances in Difference Equations*, *2019*, Article 446.

Arshed, S., Akram, G., Sadaf, M., Riaz, M. B., & Wojciechowski, A. (2023). Solitary wave behavior of (2+1)-dimensional Chaffee-Infante equation. *PLoS ONE*, *18*(1), Article e0276961.

Craster, R. V., & Sassi, R. (2018). Spectral algorithms for reaction-diffusion equations. *arXiv*. https://arxiv.org/abs/1810.07431

Demiray, S. T., & Bayrakci, U. (2021). Construction of soliton solutions for Chaffee-Infante equation. *Afyon Kocatepe University Journal of Sciences and Engineering*, *21*(5), 1046–1051.

Douglas, J., & Gunn, J. E. (1964). A general formulation of alternating direction methods. *Numerische Mathematik*, *6*, 428–453.

Fife, P. C., & McLeod, J. B. (1977). The approach of solutions of nonlinear diffusion equations to travelling front solutions. *Archive for Rational Mechanics and Analysis*, *65*, 335–361.

Mao, Y. (2018). Exact solutions to (2+1)-dimensional Chaffee-Infante equation. *Pramana*, *91*(1), Article 9.

Peaceman, D. W., & Rachford, H. H. (1959). The numerical solution of parabolic and elliptic differential equations. *Journal of the Society for Industrial and Applied Mathematics*, *3*(1), 28–41.

Rawat, A. K., Dhiman, N., & Chauhan, A. (2022). Convergence scheme and numerical approach to find the optimal solution of Chafee-Infante equation. *AIP Conference Proceedings, 2481*, Article 040025.

A NEW QUANTUM SPACE AND ITS HOPF ALGEBRA STRUCTURE

Sultan ABACI ÇELİK[1]

1. INTRODUCTION

Quantum groups and noncommutative geometry have emerged as important mathematical frameworks for extending classical concepts of symmetry, space, and differential geometry beyond the commutative setting. In classical geometry, a space can be studied through its algebra of coordinate functions, while its symmetries are described by groups acting on these functions. The passage to the quantum setting replaces, in general, the commutative algebra of functions by a noncommutative algebra. Within this algebraic viewpoint, the resulting quantum symmetries are naturally described by Hopf algebras and related quantum groups. This perspective has established a close relationship between noncommutative coordinate algebras, quantum groups, and generalized geometric structures (Drinfeld, 1987; Majid, 1995; Manin, 1988, 2018).

A fundamental idea in this development is to regard a noncommutative algebra as the algebra of coordinate functions on a quantum space. Rather than starting with a classical group and deforming its multiplication or coordinate functions, Manin proposed an approach in which quantum spaces themselves provide the basic objects and quantum groups arise as their symmetry structures. In particular, quadratic algebras can be interpreted as quantum analogues of linear spaces, with the

[1] Doç. Dr., Yıldız Teknik Üniversitesi, Fen-Edebiyat Fakültesi, Matematik Bölümü, ORCID: 0000-0003-3465-8209.

classical commutation relations replaced by deformation-dependent quadratic relations (Manin, 1988, 2018). This viewpoint is especially useful for constructing explicit examples of quantum spaces and for determining the quantum groups that preserve their defining relations.

The algebraic structure required to formulate quantum symmetries is provided by Hopf algebras. A Hopf algebra combines an associative algebra structure with a compatible coalgebra structure and an antipode, thereby providing an algebraic analogue of multiplication, identity, and inverse operations in classical groups. This framework is particularly suitable for quantum groups because the coordinate algebras of quantum groups are typically noncommutative and, in general, noncocommutative. The systematic development of Hopf algebras, matrix quantum groups, quantum enveloping algebras, and related constructions has therefore become a central part of quantum group theory (Drinfeld, 1987; Majid, 1995).

The relationship between quantum spaces and their symmetry quantum groups has also been investigated from the perspective of differential structures. Once the coordinate algebra of a space becomes noncommutative, the construction of differential forms cannot generally be obtained by simply imposing the classical commutation rules. Instead, the algebra of differential forms must be deformed consistently with the relations of the underlying coordinate algebra. Woronowicz developed a general theory of differential calculus on quantum groups and introduced the framework of bicovariant differential calculi, in which differential forms and exterior derivatives are compatible with the Hopf algebraic structure (Woronowicz, 1987, 1989).

The relationship between the present construction and the existing three-dimensional quantum-space literature is therefore

twofold. On the one hand, standard quantum Euclidean spaces such as $\mathbb{R}_q^3$ provide important reference models for three-dimensional noncommutative geometry and differential calculus (Cerchiai et al., 2000; Wachter, 2007; Celik, 1998; Celik & Celik, 2000; Celik et al., 2009). On the other hand, the work of Celik and collaborators demonstrates that alternative deformation principles, including supersymmetric, graded, contracted, and nonstandard constructions, can lead to genuinely new Hopf-algebraic quantum spaces (Celik, 2016, 2020, 2021; Celik & Temli, 2019). The proposed $\mathbb{C}_q^3$ is situated within this broader landscape while focusing on an ordinary three-coordinate, ungraded quantum space with a new defining deformation.

In this work, we introduce a new three-dimensional quantum space and investigate its Hopf algebraic and covariant structures together with its symmetry group. The corresponding quantum algebra $O(M_q(3,\mathbb{C}))$ is then investigated through its coactions on both the coordinate algebra and the q-deformed exterior algebra. The entries of the matrix $T = (t_{ij})$ are required to satisfy relations determined by the condition that the coactions preserve the defining relations of the quantum space and its exterior algebra. In this way, the quantum group is obtained as a symmetry object of the proposed quantum space, in accordance with the general philosophy of quantum groups as symmetries of noncommutative spaces (Manin, 1988, 2018).

The remainder of this chapter is organized as follows. Section 2 provides a brief review of the basic notions and properties of algebras, coalgebras, bialgebras, and Hopf algebras that are used in the subsequent construction. Section 3 contains the main results of the chapter. In Section 3.1, we introduce the new three-dimensional quantum space, discuss its quadratic defining relations and classical limit, and construct the associated q-deformed exterior algebra. Section 3.2 is devoted to the

construction and verification of the coproduct, counit, and antipode, establishing the Hopf algebra structure of the proposed quantum space. In Section 4, we introduce a new quantum bialgebra $O(M_q(3,\mathbb{C}))$, determine its coactions on the quantum coordinate and exterior algebras.

2. A BRIEF OVERVIEW OF THE DEFINITION OF A HOPF ALGEBRA

We first recall some basic definitions and properties of Hopf algebras that will be used throughout this work.

Definition 2.1. Let K be a field. An associative unital algebra over K is a K-vector space A equipped with two linear maps $m: A \otimes A \to A$, $\eta: K \to A$, called the multiplication and unit maps, respectively, satisfying

$$m \circ (m \otimes id) = m \circ (id \otimes m),$$

$$m \circ (\eta \otimes id) = m \circ (id \otimes \eta) = id_A.$$

For $a, b \in A$, we write $m(a \otimes b) = a \cdot b$ and $\eta(1) = 1_A$.

Definition 2.2. A coalgebra over K is a K-vector space A equipped with two linear maps $\Delta: A \to A \otimes A$, $\varepsilon: A \to K$, called the coproduct and counit, respectively, satisfying

$$(\Delta \otimes id) \circ \Delta = (id \otimes \Delta) \circ \Delta,$$

$$(\varepsilon \otimes id) \circ \Delta = (id \otimes \varepsilon) \circ \Delta = id.$$

Definition 2.3. A bialgebra over K is a vector space A that is simultaneously an associative unital algebra and a coalgebra, such that the coproduct and counit are algebra homomorphisms.

Equivalently, the maps $\Delta: A \to A \otimes A$ and $\varepsilon: A \to K$ are morphisms of algebras.

Definition 2.4. A Hopf algebra over K is a bialgebra A together with a linear map $\kappa: A \to A$, called the coinverse or antipode, satisfying

$$m \circ (\kappa \otimes id) \circ \Delta = m \circ (id \otimes \kappa) \circ \Delta = \eta \circ \varepsilon.$$

Thus, a Hopf algebra may be viewed as a bialgebra equipped with an antipode. We denote a Hopf algebra by $(A, m, \eta, \Delta, \varepsilon, \kappa)$.

Theorem 2.5. Let A be a Hopf algebra with antipode κ. Then κ is an algebra antihomomorphism and a coalgebra anti-homomorphism. In particular, for all $a, b \in A$,

$$\kappa(a \cdot b) = \kappa(b) \cdot \kappa(a), \quad \kappa(1_A) = 1_A,$$

$$\Delta\big(\kappa(a)\big) = (\kappa \otimes \kappa) \circ \tau \circ \Delta(a),$$

where $\tau: A \otimes A \to A \otimes A$ is defined by $\tau(a \otimes b) = b \otimes a$.

Moreover, $\varepsilon \circ \kappa = \varepsilon$. If the antipode is bijective, then

$$\kappa^{-1}(ab) = \kappa^{-1}(b)\kappa^{-1}(a).$$

In the theory of quantum groups, the algebra A is generally noncommutative, while its coproduct need not be cocommutative. This noncommutative and noncocommutative structure provides the algebraic framework for describing quantum deformations of classical groups and spaces.

3. A NEW QUANTUM SPACE AND ITS HOPF ALGEBRA STRUCTURE

In this section, we introduce a new three-dimensional quantum space and determine its Hopf algebra structure.

3.1. A New 3d Quantum Space

A quantum space is described algebraically by a noncommutative coordinate algebra generated by quantum coordinates subject to quadratic relations. This viewpoint is central to Manin's approach to quantum groups and noncommutative geometry.

Definition 3.1. Let q be nonzero complex parameter. The three-dimensional quantum space is defined as the quadratic algebra

$$O(\mathbb{C}_q^3) = \mathbb{C}\langle x, y, z\rangle / I_q,$$

where $\mathbb{C}\langle x, y, z\rangle$ denotes the free associative algebra generated by x, y, and z, and I_q is the two-sided ideal generated by the quadratic relations

$$x \cdot y = y \cdot x, \quad x \cdot z = q^2 z.x, \quad y.z = z \cdot y. \tag{3.1}$$

The generators x, y, and z are interpreted as the noncommuting coordinate functions of the quantum space. The parameter q measures the deformation of the commutative coordinate algebra. In the limit $q \to 1$, the algebra $O(\mathbb{C}_q^3)$ becomes the ordinary polynomial algebra $\mathbb{C}[x, y, z]$.

Example 3.2. If we define a representation $\rho : O(\mathbb{C}_q^3) \to M_3(\mathbb{C})$ by

$$\rho(x) = \begin{pmatrix} 1 & 0 & 0 \\ 0 & 1 & 0 \\ 0 & 0 & q^2 \end{pmatrix}, \quad \rho(y) = \begin{pmatrix} q^2 & 0 & 0 \\ 1-q^2 & 1 & 0 \\ 0 & 0 & q^2 \end{pmatrix},$$

$$\rho(z) = \begin{pmatrix} 0 & 0 & 0 \\ 0 & 0 & 0 \\ 1-q^2 & 0 & 0 \end{pmatrix},$$

then we can see that ρ is a representation of the algebra $O(\mathbb{C}_q^3)$, in the sense that the matrices $\rho(\cdot)$ preserve the relations given in (3.1) according to the rule

$$\rho_{ik}(f \cdot g) = \sum_{j=1}^{3} \rho_{ij}(f) \cdot \rho_{jk}(g)\,,$$

for all $f, g \in O(\mathbb{C}_q^3)$.

The notation $\mathbb{C}\langle x, y, z\rangle$ emphasizes that the generators x, y, and z are initially free and noncommuting. The ideal I_q imposes the quadratic relations among these generators. Hence, the quantum space is completely specified by its generators and defining relations. Equivalently, one may write

$$I_q = \langle x \cdot y - y \cdot x,\ x \cdot z - q^2\, z \cdot x,\ y \cdot z - z \cdot y \rangle.$$

The quotient by I_q identifies monomials that differ by the defining commutation relations. For example, $x \cdot y$ and $y \cdot z$ can be replaced by $y \cdot x$ and $z \cdot y$, respectively, while $x \cdot z$ can be replaced by $q^2\, z \cdot x$.

Remark 3.3. Unlike the classical coordinate algebra $\mathbb{C}[x, y, z]$, the algebra $O(\mathbb{C}_q^3)$ is generally noncommutative. For generic values of q, the products $x \cdot z$ and $z \cdot x$ are distinct elements of $O(\mathbb{C}_q^3)$, although they are related by the defining relations. This noncommutativity is the essential algebraic feature of the corresponding quantum space.

Definition 3.4. Let $\Lambda(\mathbb{C}_q^3)$ denote the exterior algebra of the algebra $O(\mathbb{C}_q^3)$. Its generators θ, φ, and ϕ are assumed to satisfy the following relations:

$\Theta_i^2 = 0,$ for $i = 1,2,3,$

$$\theta \cdot \varphi = -q^{-2}\varphi \cdot \theta,\ \ \theta \cdot \phi = -\phi \cdot \theta,\ \ \varphi \cdot \phi = -q^2 \phi \cdot \varphi, \quad (3.2)$$

where $\Theta_1 = \theta, \Theta_2 = \varphi, \Theta_3 = \phi$.

The above relations define a q-deformed exterior algebra associated with $O(\mathbb{C}_q^3)$. In particular, the relations $\Theta_i^2 = 0$, for $i = 1,2,3$ are analogous to the classical relations $dx \wedge dx = 0$, etc., where dx is differential of x, etc. The remaining relations describe the q-deformed anticommutation rules among the generators. Notice that, in the limit $q \to 1$, these relations reduce to the usual anticommutation relations. Thus, $\Lambda(\mathbb{C}_q^3)$ can be regarded as a q-deformation of the classical exterior algebra of $\mathbb{C}_q^3$.

Remark 3.5. The importance of the quantum space in Manin's approach is that quantum groups can be constructed as symmetry objects acting on such noncommutative coordinate algebras. Instead of beginning with a group and deforming its coordinate functions, one may first specify the algebra of a quantum space and then determine the quantum group that preserves its defining relations. This provides an algebraic realization of quantum groups as symmetry objects of noncommutative spaces (see, Section 4).

Remark 3.6. If additional conditions are imposed, particularly the invertibility of a suitable generator, the algebra can be endowed with a bialgebra or Hopf algebra structure. The coproduct, counit, and antipode are then required to be compatible with the defining relations of the quantum space. These structures allow the quantum space to be treated within the framework of quantum groups and provide the basis for studying its covariance and differential geometry.

3.2. Hopf Algebra Structure On $O(\mathbb{C}_q^3)$

We consider the three-dimensional quantum space whose coordinate algebra is generated by x, y, and z subject to the relations below. We then introduce the coproduct, counit, and

antipode and verify that these maps give the algebra a Hopf algebra structure.

Definition 3.7 Define a linear map

$$\Delta: O(\mathbb{C}_q^3) \rightarrow O(\mathbb{C}_q^3) \otimes O(\mathbb{C}_q^3)$$

on the generators by

$$\Delta(x) = x \otimes x,$$

$$\Delta(y) = y \otimes y,$$

$$\Delta(z) = x \otimes z + z \otimes y.$$

The map Δ is extended multiplicatively to the whole algebra.

Theorem 3.8. The coproduct Δ is compatible with the defining relations of $O(\mathbb{C}_q^3)$. Hence, it is a well-defined algebra homomorphism.

Proof. For $x \cdot y = y \cdot x$, one has

$$\Delta(x)\Delta(y) = x \cdot y \otimes x \cdot y = y \cdot x \otimes y \cdot x = \Delta(y)\Delta(x).$$

For $y \cdot z = z \cdot y$, one obtains $\Delta(y)\Delta(z) = \Delta(z)\Delta(y)$.

For $x \cdot z = q^2 z \cdot x$, one obtains

$$\Delta(x)\Delta(z) = q^2\Delta(z)\Delta(x).$$

Therefore, all defining relations are preserved by Δ.

Definition 3.9. Define the counit $\varepsilon: O(\mathbb{C}_q^3) \rightarrow \mathbb{C}$ on the generators by

$$\varepsilon(x) = 1, \quad \varepsilon(y) = 1, \quad \varepsilon(z) = 0,$$

and extend ε as an algebra homomorphism.

Theorem 3.10. The maps Δ and ε satisfy the coassociativity and counit conditions. Therefore, $O(\mathbb{C}_q^3)$ is a coalgebra. In particular,

$$(\Delta \otimes id) \circ \Delta = (id \otimes \Delta)\,\Delta,$$

$$(\varepsilon \otimes id) \circ \Delta = (id \otimes \varepsilon) \circ \Delta = id.$$

Proof. For example, for z,

$$(\Delta \otimes id)\Delta(z) = x \otimes x \otimes z + x \otimes z \otimes y + z \otimes y \otimes y,$$

$$(id \otimes \Delta)\Delta(z) = x \otimes x \otimes z + x \otimes z \otimes y + z \otimes y \otimes y.$$

Definition 3.11. In the Hopf algebra extension in which x and y are invertible, define the antipode κ by

$$\kappa(x) = x^{-1}, \quad \kappa(y) = y^{-1}, \quad \kappa(z) = -x^{-1} \cdot z \cdot y^{-1}.$$

The antipode is extended as an antihomomorphism.

Theorem 3.12. The algebra $O(\mathbb{C}_q^3)$, equipped with the coproduct Δ, counit ε, and antipode κ defined above, forms a Hopf algebra, provided that x and y are invertible. The antipode identities are

$$m \circ (\kappa \otimes id) \circ \Delta = m \circ (id \otimes \kappa) \circ \Delta = \eta \circ \varepsilon.$$

Proof. For x and y, these identities follow immediately from

$$\kappa(x) \cdot x = x \cdot \kappa(x) = 1 \text{ and } \kappa(y) \cdot y = y \cdot \kappa(y) = 1.$$

For z,

$$m(\kappa \otimes id)\Delta(z) = \kappa(x) \cdot z + \kappa(z) \cdot y = 0 = \varepsilon(z)1,$$

and

$$m(id \otimes \kappa)\Delta(z) = x \cdot \kappa(z) + z \cdot \kappa(y) = 0 = \varepsilon(z)1.$$

4. THE QUANTUM ALGEBRA $O(M_q(3,\mathbb{C}))$ AND ITS COACTIONS ON $O(\mathbb{C}_q^3)$ AND $\Lambda(\mathbb{C}_q^3)$

Let $M(3,\mathbb{C})$ denote the vector space of 3x3 matrices with complex entries. Each matrix $T \in M(3,\mathbb{C})$ acts naturally as a

linear transformation on the complex vector space $\mathbb{C}^3$. The classical matrix space $M(3,\mathbb{C})$ can therefore be described in terms of its coordinate functions, which generate a commutative coordinate algebra denoted by $O(M_q(3,\mathbb{C}))$.

A natural question is how this classical structure can be extended to the quantum setting. The basic idea of quantum deformation is to replace the commutative coordinate algebra by a noncommutative algebra whose defining relations depend on a deformation parameter q. In this way, the classical coordinate algebra $O(M(3,\mathbb{C}))$ is deformed into the quantum coordinate algebra $O(M_q(3,\mathbb{C}))$. The noncommutativity introduced by the deformation is governed by q, and the classical algebra is recovered in the undeformed limit $q \to 1$.

4.1. The Algebra $O(M_q(3,\mathbb{C}))$

Matrices with complex entries act as linear transformations on complex vector spaces. In this section, we will define the q-deformation of the algebra $O(M(3,\mathbb{C}))$.

Let $T = \begin{pmatrix} a & b & c \\ d & e & f \\ g & u & v \end{pmatrix} = (t_{ij})$ be a matrix whose entries belong to a free associative algebra, while the components of the vectors $X = (x,y,z)^t$ and $\Theta = (\theta,\varphi,\phi)^t$ belong to the algebras $O(\mathbb{C}_q^3)$ and $\Lambda(\mathbb{C}_q^3)$, respectively. Consider the transformations $X' = T.X$ and $\Theta' = T.\Theta$. We also assume that $q^2 + 1 \neq 0$. Under these assumptions, we have the following theorem, whose proof follows directly.

Theorem 4.1. Suppose that the matrix elements of T commute with the generators of $O(\mathbb{C}_q^3)$ and $\Lambda(\mathbb{C}_q^3)$. Then a necessary and sufficient condition for the components of X' and Θ' to satisfy relations (3.1) and (3.2), respectively, is that the following relations hold:

$$
\begin{aligned}
a\cdot b &= q^2 b\cdot a, \qquad a\cdot e = e\cdot a + (q^2-1)b\cdot d,\\
a\cdot c &= c\cdot a, \qquad a\cdot f = f\cdot a + (1-q^{-2})c\cdot d,\\
a\cdot d &= d\cdot a, \qquad a\cdot u = u\cdot a + (q^2-1)b\cdot g,\\
a\cdot g &= q^2 g\cdot a, \qquad a\cdot v = v\cdot a + (1-q^{-2})c\cdot g,\\
b\cdot c &= q^{-2}c\cdot b, \quad b\cdot d = q^{-2}d\cdot b, \quad b\cdot e = e\cdot b,\\
b\cdot f &= q^{-2}f\cdot b, b\cdot g = g\cdot b, b\cdot u = q^2 u\cdot b, b\cdot v = v\cdot b,\\
c\cdot d &= d\cdot c, \qquad c\cdot e = e\cdot c + (q^2-1)b\cdot f,\\
c\cdot f &= f\cdot c, \qquad c\cdot u = q^2 u\cdot c + (q^2-1)b\cdot v,\\
c\cdot g &= q^2 g\cdot c, \qquad c\cdot v = q^2 v\cdot c, \qquad (4.1)\\
d\cdot e &= q^2 e\cdot d, \quad d\cdot f = f\cdot d, \quad d\cdot g = g\cdot d,\\
d\cdot u &= q^2 u\cdot d, \quad d\cdot v = v\cdot d,\\
e\cdot f &= q^{-2}f\cdot e, \quad e\cdot g = g\cdot e + (q^{-2}-1)d\cdot u,\\
e\cdot u &= u\cdot e, \qquad e\cdot v = v\cdot e + (q^{-2}-1)f\cdot u,\\
f\cdot u &= q^2 u\cdot f, \quad f\cdot g = q^2 g\cdot f + (1-q^2)d\cdot v,\\
f\cdot v &= v\cdot f,\\
g\cdot u &= q^2 u\cdot g, \quad g\cdot v = v\cdot g, \quad u\cdot v = q^{-2}v\cdot u.
\end{aligned}
$$

Definition 4.2. The algebra $O(M_q(3,\mathbb{C}))$ is defined as the quotient of the free algebra $\mathbb{C}[a,b,c,d,e,f,g,u,v]$ by the two-sided ideal J_q generated by the relations (4.1) in Theorem 4.1.

4.2. Bialgebra Structure on $O(M_q(3,\mathbb{C}))$

The algebra $O(M_q(3,\mathbb{C}))$ introduced in the previous section admits a natural bialgebra structure. This structure is determined by the coproduct and counit maps, which are defined on the generators of the algebra and extended multiplicatively.

Definition 4.3. The coproduct

$$\Delta: O\left(M_q(3,\mathbb{C})\right) \rightarrow O\left(M_q(3,\mathbb{C})\right) \otimes O\left(M_q(3,\mathbb{C})\right)$$

is defined on the generators $t_{ij}, 1 \leq i,j \leq 3$, by

$$\Delta(t_{ij}) = \sum_{k=1}^{3} t_{ik} \otimes t_{kj},$$

and the counit $\varepsilon: O(M_q(3,\mathbb{C})) \rightarrow \mathbb{C}$ is given by

$$\varepsilon(t_{ij}) = \delta_{ij}.$$

The compatibility of these maps with the defining relations of $O(M_q(3,\mathbb{C}))$ leads to the following result.

Theorem 4.4. The maps Δ and ε are well defined on the algebra $O(M_q(3,\mathbb{C}))$. Moreover, they satisfy
$(\Delta \otimes id) \circ \Delta = (id \otimes \Delta) \circ \Delta, \ (\varepsilon \otimes id) \circ \Delta = (id \otimes \varepsilon) \circ \Delta = id.$

Consequently, $(O(M_q(3,\mathbb{C})), \Delta, \varepsilon)$ is a bialgebra.

Proof. It is sufficient to verify the required identities on the generators t_{ij}. For the coproduct,

$$(\Delta \otimes id)\Delta(t_{ij}) = \sum_{k,l=1}^{3} t_{il} \otimes t_{lk} \otimes t_{kj},$$

whereas

$$(id \otimes \Delta)\Delta(t_{ij}) = \sum_{k,l=1}^{3} t_{ik} \otimes t_{kl} \otimes t_{lj}.$$

After relabelling the summation indices, these expressions coincide. Similarly,

$$(\varepsilon \otimes id)\Delta(t_{ij}) = \sum_{k=1}^{3} \varepsilon(t_{ik}) t_{kj} = t_{ij},$$

and

$$(id \otimes \varepsilon)\Delta(t_{ij}) = \sum_{k=1}^{3} t_{ik} \varepsilon(t_{kj}) = t_{ij}.$$

Thus, the coproduct is coassociative and the counit identities hold. Hence $O(M_q(3,\mathbb{C}))$ is a bialgebra.

4.3. Coactions on $O(\mathbb{C}_q^3)$ and $\Lambda(\mathbb{C}_q^3)$

The bialgebra structure established above allows us to introduce a natural left coaction of $O\left(M_q(3,\mathbb{C})\right)$ on the coordinate algebra of the quantum space $O(\mathbb{C}_q^3)$. Let $x = x_1$, $y = x_2$, $z = x_3$ denote the generators of $O(\mathbb{C}_q^3)$.

Definition 4.5. A left $O(M_q(3,\mathbb{C}))$-coaction on $O(\mathbb{C}_q^3)$ is a linear map $\delta_L: O(\mathbb{C}_q^3) \to O(M_q(3,\mathbb{C}))\otimes O(\mathbb{C}_q^3)$ defined on the generators by

$$\delta_L(x_i) = \sum_{j=1}^{3} t_{ij}\otimes x_j, \quad i = 1,2,3.$$

The compatibility of this map with the defining relations of $O(\mathbb{C}_q^3)$ gives the following result.

Theorem 4.6. The map δ_L is a well-defined left coaction of the bialgebra $O(M_q(3,\mathbb{C}))$ on $O(\mathbb{C}_q^3)$. In particular, $(\Delta\otimes id)\circ\delta_L = (id\otimes\delta_L)\circ\delta_L$ and $(\varepsilon\otimes id)\circ\delta_L = id$.

Proof. For each generator x_i,

$$(\Delta\otimes id)\delta_L(x_i) = \sum_{j=1}^{3}\Delta(t_{ij})\otimes x_j = \sum_{j,k=1}^{3} t_{ik}\otimes t_{kj}\otimes x_j.$$

On the other hand,

$$(id\otimes\delta_L)\delta_L(x_i) = \sum_{j=1}^{3} t_{ij}\otimes\delta_L(x_j) = \sum_{j,k=1}^{3} t_{ij}\otimes t_{jk}\otimes x_k\,.$$

After relabelling the indices, the two expressions agree. Furthermore,

$$(\varepsilon \otimes id)\delta_L(x_i) = \sum_{j=1}^{3} \varepsilon(t_{ij})x_j = x_i.$$

Thus, δ_L satisfies the coaction axioms. The relations defining $O(\mathbb{C}_q^3)$ are preserved under δ_L by the defining relations of the algebra $O(M_q(3,\mathbb{C}))$. Therefore, the map δ_L extends uniquely to an algebra homomorphism δ_L. Hence it defines a left coaction of $O\left(M_q(3,\mathbb{C})\right)$ on $O(\mathbb{C}_q^3)$.

Definition 4.7. The coaction δ is extended to the exterior algebra by

$$\delta' : \Lambda(\mathbb{C}_q^3) \rightarrow O(GL_q(3)) \otimes \Lambda(\mathbb{C}_q^3),$$

where $\delta'(\Theta_i) = \Sigma_{j=1}{}^{3}\, t_{ij} \otimes \Theta_j$.

Theorem 4.8. The algebra generated by the entries t_{ij} of T, subject to the relations obtained from the invariance of the defining relations of $O(\mathbb{C}_q^3)$ and $\Lambda(\mathbb{C}_q^3)$ under the coactions δ and δ', defines the coordinate algebra of $M_q(3,\mathbb{C})$.

More precisely, the relations among the generators t_{ij} are uniquely determined by requiring $\delta(R) = 0$ for every defining relation R of $O(\mathbb{C}_q^3)$, and $\delta'(\kappa) = 0$ for every defining relation κ of $\Lambda(\mathbb{C}_q^3)$. Consequently, $O(M_q(3,\mathbb{C}))$ acts covariantly on both the quantum coordinate algebra $O(\mathbb{C}_q^3)$ and its exterior algebra $\Lambda(\mathbb{C}_q^3)$.

5. CONCLUSION

In this paper, we introduced a new three-dimensional quantum space $O(\mathbb{C}_q^3)$ and investigated its fundamental algebraic and Hopf-algebraic structures. A Hopf algebra structure compatible with the defining relations of $O(\mathbb{C}_q^3)$ was constructed.

The coproduct, counit, and antipode were explicitly defined and their compatibility conditions were verified. A distinctive feature of the resulting Hopf algebra is the non-primitive coproduct of the generator z, $\Delta(z) = x \otimes z + z \otimes y$, which differs from the usual primitive coproduct encountered in classical and some quantum algebraic constructions. This structure provides an explicit example of a three-dimensional quantum space equipped with a nontrivial coalgebraic structure.

We also considered a q-deformed exterior algebra associated with $O(\mathbb{C}_q^3)$. The defining relations among the exterior generators reduce to the classical anticommutation relations in the limit. Furthermore, the quantum algebra $O(M_q(3,\mathbb{C}))$ was introduced through its coactions on both the quantum coordinate algebra and the associated exterior algebra.

The results obtained in this paper provide the algebraic foundation for a more detailed investigation of the differential geometry of the newly introduced quantum space. In particular, a natural continuation of the present work is the construction of a differential calculus on $O(\mathbb{C}_q^3)$. Such a study would involve determining the commutation relations between the generators x, y, z and their differentials, constructing the corresponding exterior algebra systematically, and identifying the associated differential operators and their algebraic properties. The compatibility of the differential calculus with the Hopf algebra structure and the $O(M_q(3,\mathbb{C}))$-coaction would also provide an important aspect of this investigation.

A forthcoming study will therefore focus specifically on the differential calculus on $O(\mathbb{C}_q^3)$. Building on the Hopf algebra and exterior structures established here, that work will investigate the differential relations, exterior derivative, higher-degree differential forms, and covariance properties associated with the proposed quantum space. In particular, the aim is to develop a

consistent noncommutative differential geometry for $O(\mathbb{C}_q^3)$ and to examine how its differential structure interacts with the Hopf algebraic and $O(M_q(3,\mathbb{C}))$-covariant structures obtained in the present chapter. This continuation will provide a natural extension of the present algebraic construction and will contribute to a more complete geometric understanding of the new quantum space.

REFERENCES

Celik, S. (1998). Differential geometry of the q-superplane. Journal of Physics A: Mathematical and General 31, 9695-9701.

Celik, S.A., & Celik, S. (2000). Differential geometry of the q-plane. International Journal of Modern Physics A, 15, 3237-3243.

Celik, S., Ozkan, E. M., & Yasar, E. (2009). Cartan calculus on the quantum space $\mathbb{R}_q^3$. Turkish Journal of Mathematics, 33(1), 75–83. doi:10.3906/mat-0802-23

Celik, S. (2016). Bicovariant differential calculus on the quantum superspace $\mathbb{R}_q^{1|2}$. Journal of Algebra and Its Applications, 15(9). doi:10.1142/S0219498816501723

Celik, S. (2020). Hopf algebra structure on superspace $SP_q^{2|1}$. Hacettepe Journal of Mathematics and Statistics, 49(2), 777–783. doi:10.15672/hujms.499848

Celik, S. (2021). On q- and h-deformations of 3d-superspaces. Turkish Journal of Mathematics, 45(1), 346–359. doi:10.3906/mat-1907-80

Celik, S., & Temli, I. (2019). Covariant differential calculus on $SP_h^{2|1}$. Turkish Journal of Mathematics, 43(2), 916–929. doi:10.3906/mat-1812-92

Cerchiai, B. L., Madore, J., Schraml, S., & Wess, J. (2000). Structure of the three-dimensional quantum Euclidean space. European Physical Journal C, 16, 99–105.

Drinfeld, V. G. (1987). Quantum groups. In Proceedings of the International Congress of Mathematicians, Berkeley, 1986 (pp. 798–820). Providence, RI: American Mathematical Society.

Majid, S. (1995). Foundations of quantum group theory. Cambridge, England: Cambridge University Press.

Manin, Y. I. (1988). Quantum groups and non-commutative geometry. Montréal, Canada: Centre de recherches mathématiques.

Manin, Y. I. (2018). Quantum groups and noncommutative geometry (2nd ed.). Cham, Switzerland: Springer.

Wachter, H. (2007). Analysis on q-deformed quantum spaces. International Journal of Modern Physics A, 22(1), 79–128. doi:10.1142/S0217751X07034155

Woronowicz, S. L. (1987). Twisted $SU(2)$ group: An example of a non-commutative differential calculus. Publications of the Research Institute for Mathematical Sciences, 23(1), 117–181. doi:10.2977/PRIMS/1195176848

Woronowicz, S. L. (1989). Differential calculus on compact matrix pseudogroups (quantum groups). Communications in Mathematical Physics, 122(1), 125–170. doi:10.1007/BF01221411

WEYL PROJECTIVE CURVATURE ON METALLIC RIEMANNIAN SPACE FORMS

Semra ZEREN[1]

1. INTRODUCTION

Let $(\widetilde{M}^n, J, g)$ be an n-dimensional Riemannian manifold, $n \geq 2$, endowed with a metallic structure J; see Blaga and Nannicini (2019), Chen, Choudhary, and Perween (2025), Gezer and Karaman (2015), and Hreţcanu and Crasmareanu (2013) for background. Related submanifold geometry for manifolds endowed with other tensor structures is considered, for example, by Zeren and Yıldız (2026). The metallic structure is determined by

$$J^2 = pJ + q\mathrm{Id}, \qquad p, q \in \mathbb{N}^*, \tag{1}$$

and is assumed to be compatible with the metric in the sense that

$$g(JX, Y) = g(X, JY) \tag{2}$$

for all vector fields X, Y. When

$$\widetilde{\nabla} J = 0, \tag{3}$$

the metallic Riemannian manifold is called locally decomposable.

The purpose of this chapter is to calculate the Weyl projective curvature tensor on a locally decomposable metallic Riemannian space form. The starting point is the explicit expression of the Riemann curvature tensor and the Ricci tensor

[1] Asst. Prof. Dr., Sivas Science and Technology Univesity, Faculty of Engineering and Natural Sciences, Department of Fundamental Engineering Sciences, ORCID: 0000-0003-0083-3507

associated with a constant metallic sectional curvature. The calculation is then organized in two steps:

1. derive an explicit formula for the Weyl projective curvature tensor;
2. analyze the condition $\mathcal{P} = 0$ using the eigenvalues of J.

Throughout the chapter, all calculations are performed with the curvature convention fixed in Section 2.

2. GEOMETRIC SETTING AND CONVENTIONS

Let $\widetilde{\nabla}$ denote the Levi–Civita connection of g. We use the curvature convention

$$\tilde{R}(X,Y)Z = \widetilde{\nabla}_X\widetilde{\nabla}_Y Z - \widetilde{\nabla}_Y\widetilde{\nabla}_X Z - \widetilde{\nabla}_{[X,Y]}Z. \tag{4}$$

For a local orthonormal frame $\{e_1, \dots, e_n\}$, the Ricci tensor is defined by

$$\tilde{S}(X,Y) = \sum_{i=1}^{n} g\left(\tilde{R}(e_i,X)Y, e_i\right). \tag{5}$$

The Ricci operator $\tilde{Q}$ is defined by

$$g\left(\tilde{Q}X, Y\right) = \tilde{S}(X,Y). \tag{6}$$

Throughout the chapter we assume $n \geq 2$.

We use the following Weyl projective curvature tensor (Mishra, 1969):

$$\tilde{\mathcal{P}}(X,Y)Z = \tilde{R}(X,Y)Z - \frac{1}{n-1}\left\{\tilde{S}(Y,Z)X - \tilde{S}(X,Z)Y\right\}. \tag{7}$$

Related projective-curvature notions in Kähler geometry include the H-projective tensor studied by Mishra (1969); curvature tensor calculations for Riemannian submersions are discussed by Karataş, Zeren, and Altın (2024).

3. METALLIC RIEMANNIAN SPACE FORMS

Assume that $(\widetilde{M}^n, J, g)$ is a locally decomposable metallic Riemannian space form with constant metallic sectional curvature c. For convenience, set

$$\kappa = \frac{c}{3q}, \qquad \tau = \sum_{i=1}^{n} g\,(Je_i, e_i). \tag{8}$$

Following the constant metallic sectional-curvature formula of Şahin, Şahin, and Erdoğan (2026), we write the Riemann curvature tensor of the metallic Riemannian space form as

$$\begin{aligned}\tilde{R}(X,Y)Z = \kappa\{&qg(Y,Z)X - 2g(X,JZ)JY + pg(X,JZ)Y \\ &+pg(X,Z)JY - qg(X,Z)Y + 2g(Y,JZ)JX \\ &-pg(Y,JZ)X - pg(Y,Z)JX\}.\end{aligned} \tag{9}$$

Introduce the coefficients

$$\alpha = nq - 3q - p\tau, \qquad \beta = 2\tau - np. \tag{10}$$

Then the Ricci tensor is

$$\tilde{S}(X,Y) = \kappa\{\alpha g(X,Y) + \beta g(X,JY)\}. \tag{11}$$

Since J is self-adjoint with respect to g, (11) gives

$$\tilde{Q}X = \kappa(\alpha X + \beta JX). \tag{12}$$

4. EXPLICIT COMPUTATION OF THE WEYL PROJECTIVE TENSOR

We now calculate $\tilde{\mathcal{P}}$ step by step.

4.1. The Ricci Correction Term

From (11),

$$\tilde{S}(Y,Z) = \kappa\{\alpha g(Y,Z) + \beta g(Y,JZ)\}, \tag{13}$$

$$\tilde{S}(X,Z) = \kappa\{\alpha g(X,Z) + \beta g(X,JZ)\}. \tag{14}$$

Therefore,

$$\tilde{S}(Y,Z)X - \tilde{S}(X,Z)Y = \kappa\{\alpha[g(Y,Z)X - g(X,Z)Y] + \beta[g(Y,JZ)X - g(X,JZ)Y]\}. \quad (15)$$

Substituting (9) and (15) into (7), we obtain

$$\tilde{\mathcal{P}}(X,Y)Z = \kappa\{qg(Y,Z)X - 2g(X,JZ)JY + pg(X,JZ)Y + pg(X,Z)JY - qg(X,Z)Y + 2g(Y,JZ)JX - pg(Y,JZ)X - pg(Y,Z)JX - \frac{\alpha}{n-1}[g(Y,Z)X - g(X,Z)Y] - \frac{\beta}{n-1}[g(Y,JZ)X - g(X,JZ)Y]\}. \quad (16)$$

4.2. Simplification of the Coefficients

The coefficient of $g(Y,Z)X - g(X,Z)Y$ is

$$q - \frac{\alpha}{n-1} = q - \frac{nq - 3q - p\tau}{n-1} = \frac{2q+p\tau}{n-1}. \quad (17)$$

The terms involving $g(X,JZ)Y - g(Y,JZ)X$ have coefficient

$$p + \frac{\beta}{n-1} = p + \frac{2\tau - np}{n-1} = \frac{2\tau-p}{n-1}. \quad (18)$$

The remaining terms containing JX and JY are not affected by the Ricci correction. Consequently, we obtain the following theorem.

Theorem 1 (Explicit Weyl projective tensor). *Let $(\widetilde{M}^n, J, g)$ be a locally decomposable metallic Riemannian space form with constant metallic sectional curvature c. Under the conventions (4)–(7), its Weyl projective curvature tensor is*

$$\tilde{\mathcal{P}}(X,Y)Z = \frac{c}{3q}\{$$
$$\frac{2q+p\tau}{n-1}[g(Y,Z)X - g(X,Z)Y]$$
$$+\frac{2\tau-p}{n-1}[g(X,JZ)Y - g(Y,JZ)X]$$
$$-2g(X,JZ)JY + 2g(Y,JZ)JX$$
$$+pg(X,Z)JY - pg(Y,Z)JX\}. \quad (19)$$

4.3. The (0,4)-Form

Define

$$\tilde{\mathcal{P}}(X,Y,Z,W) = g\big(\tilde{\mathcal{P}}(X,Y)Z,W\big). \quad (20)$$

Using $g(JX,W) = g(X,JW)$, Theorem 1 gives

$$\tilde{\mathcal{P}}(X,Y,Z,W) = \frac{c}{3q}\{$$
$$\frac{2q+p\tau}{n-1}[g(Y,Z)g(X,W) - g(X,Z)g(Y,W)]$$
$$+\frac{2\tau-p}{n-1}[g(X,JZ)g(Y,W) - g(Y,JZ)g(X,W)]$$
$$-2g(X,JZ)g(Y,JW) + 2g(Y,JZ)g(X,JW)$$
$$+pg(X,Z)g(Y,JW) - pg(Y,Z)g(X,JW)\}. \quad (21)$$

5. TRACE PROPERTY

The Weyl projective tensor in (7) has vanishing Ricci contraction. Indeed, let $\{e_1,\dots,e_n\}$ be a local orthonormal frame. Then

$$\sum_{i=1}^{n} g\left(\tilde{\mathcal{P}}(e_i, Y)Z, e_i\right) = \tilde{S}(Y, Z)$$

$$-\frac{1}{n-1}\sum_{i=1}^{n}\left[\tilde{S}(Y, Z)g(e_i, e_i) - \tilde{S}(e_i, Z)g(Y, e_i)\right]$$

$$= \tilde{S}(Y, Z) - \frac{1}{n-1}\left[n\tilde{S}(Y, Z) - \tilde{S}(Y, Z)\right]$$

$$= 0. \tag{22}$$

Hence

$$\mathrm{Ric}_{\tilde{\mathcal{P}}} = 0. \tag{23}$$

6. PROJECTIVELY FLAT METALLIC SPACE FORMS

We now analyze the condition

$$\tilde{\mathcal{P}} = 0. \tag{24}$$

The eigenvalues of J are the roots of

$$\lambda^2 - p\lambda - q = 0. \tag{25}$$

Thus,

$$\sigma_{\pm} = \frac{p \pm \sqrt{p^2 + 4q}}{2}, \tag{26}$$

and

$$\sigma_{+} + \sigma_{-} = p, \qquad \sigma_{+}\sigma_{-} = -q. \tag{27}$$

Since J is self-adjoint, an orthonormal eigenframe may be chosen locally. Let X, Y be orthogonal unit eigenvectors satisfying

$$JX = \lambda X, \qquad JY = \mu Y. \tag{28}$$

Putting $Z = Y$ in (19), we have

$$\tilde{\mathcal{P}}(X, Y)Y = \frac{c}{3q}F(\lambda, \mu)X, \tag{29}$$

where

$$F(\lambda,\mu)=\frac{2q+p\tau}{n-1}-\frac{2\tau-p}{n-1}\mu+(2\mu-p)\lambda. \tag{30}$$

For two distinct eigenvalues, projective flatness implies

$$F(\lambda,\mu)=F(\mu,\lambda)=0.$$

Subtracting these equations gives

$$F(\lambda,\mu)-F(\mu,\lambda)=-\frac{np-2\tau}{n-1}(\lambda-\mu). \tag{31}$$

Therefore, if $\lambda\neq\mu$, then

$$\tau=\frac{np}{2}. \tag{32}$$

Using (27) and (32), one obtains

$$F(\sigma_{+},\sigma_{-})=-\frac{(n-2)(p^2+4q)}{2(n-1)}. \tag{33}$$

Consequently, for $n>2$ and $c\neq 0$,

$$F(\sigma_{+},\sigma_{-})\neq 0, \tag{34}$$

because $p^2+4q>0$. Hence a nontrivial metallic structure carrying both metallic eigenvalues cannot be projectively flat.

Proposition 2. *Assume $n>2$ and $c\neq 0$. If both distinct metallic eigenvalues σ_{+} and σ_{-} occur in the spectrum of J, then $\tilde{\mathcal{P}}\neq 0$.*

Proof. Choose orthogonal unit eigenvectors X,Y associated with σ_{+} and σ_{-}, and write $\lambda=\sigma_{+}$, $\mu=\sigma_{-}$. Since $\lambda\neq\mu$, consider two cases.

If $\tau\neq np/2$, then (31) gives

$$F(\lambda,\mu)\neq F(\mu,\lambda).$$

Thus at least one of these two values is nonzero. Applying (29) to (X,Y) and to (Y,X) shows that at least one of $\tilde{\mathcal{P}}(X,Y)Y$ and $\tilde{\mathcal{P}}(Y,X)X$ is nonzero.

If $\tau = np/2$, then (33) gives

$$\tilde{\mathcal{P}}(X,Y)Y = -\frac{c}{3q}\,\frac{(n-2)(p^2+4q)}{2(n-1)}X,$$

which is nonzero because $n > 2$, $c \neq 0$, and $p, q > 0$. □

6.1. Scalar Metallic Structures

Suppose that

$$J = \lambda \mathrm{Id}. \tag{35}$$

Then λ satisfies

$$\lambda^2 = p\lambda + q. \tag{36}$$

Substituting $J = \lambda$Id into (9) and using (36), we obtain

$$\tilde{R}(X,Y)Z = c[g(Y,Z)X - g(X,Z)Y]. \tag{37}$$

Indeed, the coefficients of $g(Y,Z)X$ and $g(X,Z)Y$ inside the braces in (9) become, respectively, $q + 2\lambda^2 - 2p\lambda = 3q$ and $-2\lambda^2 + 2p\lambda - q = -3q$, by (36). The Ricci convention (5) then gives

$$\tilde{S}(X,Y) = (n-1)c\, g(X,Y). \tag{38}$$

Substituting these curvature and Ricci tensors into (7) yields

$$\tilde{\mathcal{P}}(X,Y)Z = 0. \tag{39}$$

Remark 3. The conclusion in (39) is also immediate from the fact that, when $J = \lambda$Id, the metallic Riemann tensor reduces to a constant-curvature-type tensor and the corresponding Ricci correction removes its projective part.

6.2. The Flat Case

If $c = 0$, then $\kappa = 0$ and consequently

$$\tilde{R} = 0, \qquad \tilde{S} = 0, \qquad \tilde{\mathcal{P}} = 0. \tag{40}$$

7. MAIN PROJECTIVE-FLATNESS STATEMENT

The preceding calculations can be summarized as follows.

Theorem 4. *Let $(\widetilde{M}^n, J, g)$ be a locally decomposable metallic Riemannian space form with $p, q > 0$ and constant metallic sectional curvature c. Assume that the spectrum of J is considered through the two metallic roots σ_+ and σ_-. Then:*

(i) *if $c = 0$, then $\tilde{\mathcal{P}} = 0$;*

(ii) *if $n = 2$, then $\tilde{\mathcal{P}} \equiv 0$;*

(iii) *if $n > 2$, $c \neq 0$, and both σ_+ and σ_- occur, then $\tilde{\mathcal{P}} \neq 0$;*

(iv) *if $J = \lambda \mathrm{Id}$ with $\lambda^2 = p\lambda + q$, then $\tilde{\mathcal{P}} = 0$.*

In particular, for $n > 2$ and $c \neq 0$, the simultaneous occurrence of both metallic eigenvalues obstructs projective flatness.

8. SPECIAL CASES

8.1. The Golden Case

The golden structure is the special case of the metallic structure obtained by choosing $p = q = 1$. In this case the eigenvalues of structure J are

$$\sigma_{\pm} = \frac{1 \pm \sqrt{5}}{2}.$$

Formula (19) becomes

$$\begin{aligned} \tilde{\mathcal{P}}(X,Y)Z = \frac{c}{3}\{&\frac{2+\tau}{n-1}[g(Y,Z)X - g(X,Z)Y] \\ &+\frac{2\tau-1}{n-1}[g(X,JZ)Y - g(Y,JZ)X] \\ &-2g(X,JZ)JY + 2g(Y,JZ)JX \\ &+g(X,Z)JY - g(Y,Z)JX\}. \end{aligned} \tag{41}$$

8.2. Einstein Condition

From (12),

$$\tilde{Q} = \kappa(\alpha \mathrm{Id} + \beta J), \qquad \kappa = \frac{c}{3q}, \qquad \beta = 2\tau - np.$$

Thus, $\tilde{Q}$ is a scalar multiple of the identity exactly when at least one of $c = 0$, $\tau = np/2$, or $J = \lambda \mathrm{Id}$ holds. If $c \neq 0$ and both distinct metallic eigenvalues occur, then J is nonscalar, so the Einstein condition is equivalent to $\beta = 0$, or $\tau = np/2$. If $c = 0$, then $\tilde{Q} = 0$ and the metric is Einstein. If $J = \lambda \mathrm{Id}$, then $\tilde{Q} = \kappa(\alpha + \beta\lambda)\mathrm{Id}$, so it is Einstein without requiring $\tau = np/2$.

On the nonflat branch with both metallic eigenvalues present, substituting $\tau = np/2$ into (19) makes the coefficient of $g(X, JZ)Y - g(Y, JZ)X$ equal to p. Therefore,

$$\begin{aligned}\tilde{\mathcal{P}}_{\mathrm{Ein}}(X,Y)Z = \frac{c}{3q}\{ & \\ \frac{2q + \frac{np^2}{2}}{n-1}[g(Y,Z)X - g(X,Z)Y] & \\ +p[g(X,JZ)Y - g(Y,JZ)X] & \\ -2g(X,JZ)JY + 2g(Y,JZ)JX & \\ +pg(X,Z)JY - pg(Y,Z)JX\}. & \qquad (42)\end{aligned}$$

9. CONCLUSION

In this chapter, the Weyl projective curvature tensor of a locally decomposable metallic Riemannian space form was calculated explicitly. The formula depends on the metallic parameters p, q, the constant metallic sectional curvature c, the dimension n, the metric, and the trace of the metallic structure.

The main formula is (19). It is obtained by substituting the metallic Riemann and Ricci tensors into the fixed Weyl projective

definition. The tensor has vanishing Ricci contraction, as shown in (23). The eigenvalue calculation further shows that a nonzero constant metallic sectional curvature together with the simultaneous occurrence of both metallic eigenvalues prevents projective flatness in dimensions $n > 2$.

REFERENCES

Blaga, A. M., & Nannicini, A. (2019). On curvature tensors of Norden and metallic pseudo-Riemannian manifolds. *Complex Manifolds, 6,* 150–159. https://doi.org/10.1515/coma-2019-0008

Chen, B.-Y., Choudhary, M. A., & Perween, A. (2025). Recent advances in metallic Riemannian geometry: A comprehensive review. *Tamkang Journal of Mathematics, 56*(3), 249–290. https://doi.org/10.5556/j.tkjm.56.2025.5405

Gezer, A., & Karaman, Ç. (2015). On metallic Riemannian structures. *Turkish Journal of Mathematics, 39*(6), 954–962. https://doi.org/10.3906/mat-1504-50

Hreţcanu, C. E., & Crasmareanu, M. (2013). Metallic structures on Riemannian manifolds. *Revista de la Unión Matemática Argentina, 54*(2), 15–27.

Karataş, E., Zeren, S., & Altın, M. (2024). Geometric analysis of Riemannian submersions: Curvature tensors and total umbilic fibers. *Konuralp Journal of Mathematics,* 12(2), 158–171. https://dergipark.org.tr/en/pub/konuralpjournalmath/article/1524680

Mishra, R. S. (1969). H-projective curvature tensor in Kähler manifold. *Proceedings of the National Institute of Sciences,* New Delhi.

Şahin, F., Şahin, B., & Erdoğan, F. E. (2026). Metallic Riemannian space forms. *Hacettepe Journal of Mathematics and Statistics,* 55(5), 2188–2200. https://doi.org/10.15672/hujms.1829922

Zeren, S., & Yıldız, A. (2026). Submanifolds of almost potent manifolds. *Facta Universitatis, Series: Mathematics and Informatics, 41,* 443–454.

MATEMATİKTE GÜNCEL KONULAR VE AKADEMİK DEĞERLENDİRMELER

yaz
yayınları

YAZ Yayınları
M.İhtisas OSB Mah. 4A Cad. No:3/3
İscehisar / AFYONKARAHİSAR
Tel : (0 531) 880 92 99
yazyayinlari@gmail.com • www.yazyayinlari.com